Anna Vaskuri

Multi-Wavelength Setup Based on Lasers for Characterizing Optical Detectors and Materials

School of Electrical Engineering

Thesis submitted for examination for the degree of Master of Science in Technology.

Espoo 7.3.2014

Thesis supervisor:

Prof. Erkki Ikonen

Thesis advisors:

D.Sc. (Tech.) Petri Kärhä

M.Sc. (Tech.) Timo Dönsberg

Aalto University
School of Electrical
Engineering

AALTO UNIVERSITY
SCHOOL OF ELECTRICAL ENGINEERING

ABSTRACT OF THE
MASTER'S THESIS

Author: Anna Vaskuri

Title: Multi-Wavelength Setup Based on Lasers for Characterizing Optical Detectors and Materials

Date: 7.3.2014 Language: English Number of pages: 8+57

Department of Signal Processing and Acoustics

Professorship: Measurement Science and Technology Code: S-108

Supervisor: Prof. Erkki Ikonen

Advisors: D.Sc. (Tech.) Petri Kärhä, M.Sc. (Tech.) Timo Dönsberg

Optical detectors are used in various applications ranging from imaging devices, security systems, and robotic vision, to signaling and transmission systems. Spectral power responsivity and spatial uniformity are crucial parameters for characterizing detectors. In this thesis, a multi-wavelength setup based on lasers has been designed and constructed for these measurements. The setup directs a stable, collimated laser beam with a narrow beam diameter to a sample holder unit mounted on a high-resolution XY translation stage. Detectors can be interchanged to calibrate absolute power responsivities, or they can be scanned to obtain spatial uniformities. The measurement setup can also be used to characterize optical properties of materials, such as photoyellowing, by measuring their transmittances.

The performance of the setup was characterized by measuring the quality of the laser beam. Based on the measurements, the 8 h stability of the laser when using the laser power controller had a relative standard deviation of 0.01 %. By monitoring the stabilized beam with a monitor detector, the relative standard deviation decreased below 0.007 %. The spatial filter used in the setup was verified to smooth the beam profile, especially with diode lasers.

The setup developed improves the accuracy and repeatability of consecutive annual detector calibrations in the Metrology Research Institute. The setup enables routine scanning of the spatial uniformity in pursuance of the calibration; it can be used, e.g., to check the condition of the detector. In the material science, a combination of the ultraviolet (UV) spectrograph and the measurement setup developed enables a novel method for studying the UV radiation-induced degradation of materials with a resolution smaller than 2 nm, which is a significant improvement for earlier methods.

Keywords: Laser, Measurement setup, Optical detector calibration, Power responsivity, Spatial uniformity, UV degradation

AALTO-YLIOPISTO
SÄHKÖTEKNIIKAN KORKEAKOULU

DIPLOMITYÖN
TIIVISTELMÄ

Tekijä: Anna Vaskuri

Työn nimi: Lasereihin perustuva laitteisto optisten ilmaisimien ja materiaalien karakterisointiin

Päivämäärä: 7.3.2014 Kieli: Englanti Sivumäärä: 8+57

Signaalinkäsittelyn ja akustiikan laitos

Professuuri: Mittaustekniikka Koodi: S-108

Valvoja: Prof. Erkki Ikonen

Ohjaajat: TkT Petri Kärhä, DI Timo Dönsberg

Optisia ilmaisimia käytetään monissa sovelluksissa kuvantamislaitteista, turvajärjestelmistä sekä konenäkösovelluksista merkinanto- ja tiedonsiirtojärjestelmiin. Spektrinen tehoherkkyys ja spatiaalivaste ovat ratkaisevan tärkeitä parametreja optisten ilmaisimien karakterisoinnissa. Tässä työssä on suunniteltu ja toteutettu lasereihin perustuva laitteisto kyseisiä mittauksia varten. Mittauslaitteisto ohjaa stabiilin, kollimoidun ja halkaisijaltaan kapean lasersäteen näytepidikkeelle, joka on asennettu korkearesoluutioiselle XY-siirtimelle. Ilmaisimia voidaan vaihtaa keskenään absoluuttisen tehoherkkyyden kalibroimiseksi, tai niiden spatiaalivasteet voidaan skannata. Mittauslaitteistolla voidaan myös karakterisoida materiaalien optisia ominaisuuksia, kuten kellastumista, mittaamalla niiden transmittanssit.

Laitteiston suorituskyky karakterisoitiin mittaamalla lasersäteen laatua. Mittausten perusteella laitteiston lasersäteen 8 h stabiilisuuden suhteellinen keskihajonta oli 0.01 % käytettäessä tehosäädintä. Stabiloidun lasersäteen tarkkailu erillisellä ilmaisimella laski suhteellisen keskihajonnan alle 0.007 %:iin. Lisäksi laitteistossa käytetyn spatiaalisuodattimen todettiin tasoittavan lasersäteen profiilia, etenkin diodilaseria käytettäessä.

Kehitetty laitteisto parantaa MIKES-Aalto Mittaustekniikassa suoritettavien peräkkäisten vuotuisten ilmaisinkalibrointien tarkkuutta ja toistettavuutta. Laitteisto mahdollistaa spatiaalivasteen rutiiniskannauksen kalibroinnin yhteydessä; sillä voidaan tarkistaa esimerkiksi ilmaisimen kunto. Materiaalitieteen alalla ultravioletti (UV) spektrografin ja kehitetyn mittauslaitteiston yhdistelmä mahdollistaa uuden menetelmän tutkia UV-säteilyn aiheuttamaa materiaalien hajoamista alle 2 nm resoluutiolla, mikä on merkittävä parannus aiempiin menetelmiin verrattuna.

Avainsanat: laser, mittauslaitteisto, optisen ilmaisimen kalibrointi, tehoherkkyys, spatiaalivaste, UV-hajoaminen

Preface

This work has been conducted in the Metrology Research Institute (MRI) of Aalto University School of Electrical Engineering. The thesis was included in the UVIADEM project (UV Radiation Induced and Assisted Degradation of Materials) partly funded by the Academy of Finland.

First, I would like to thank Professor Erkki Ikonen for supervising this thesis and for the opportunity to work in the Metrology Research Institute. I am also grateful for my advisors D.Sc. (Tech.) Petri Kärhä and M.Sc. (Tech.) Timo Dönsberg for their expert guidance throughout this thesis. In addition, I would like to thank my colleagues, who helped me with practical problems in the laboratory.

Thank you for all the participants of the UVIADEM project. Special thanks go to M.Sc. (Tech.) Ville Mylläri from Tampere University of Technology (TUT), who manufactured the polystyrene samples needed in this thesis.

The greatest thanks belong to my parents and my sister for their support and patience during my studies and to Jere Liukkonen for helping me with photographing and for brightening my days.

Otaniemi, Feb. 18th 2014

Anna Vaskuri

Contents

Symbols and abbreviations

Symbols

$\epsilon(\lambda)$	molar absorption coefficient
θ	divergence angle of the fundamental TEM_{00} laser beam
Θ	divergence angle of the real laser beam
λ	wavelength
λ_e	exposure wavelength
σ	standard deviation
σ_M	standard deviation of the mean
$A(\lambda)$	absorbance
c	concentration
d	laser beam diameter
D	dose
$E(\lambda)$	spectral irradiance
f	focal length
$i(\lambda)$	spectral photocurrent
$I(\lambda)$	spectral intensity of an illuminant
l	thickness of the sample
M^2	beam quality factor
n	sample size
n_x	number of horizontal points
n_y	number of vertical points
$n_\parallel$	refractive index for the parallel ray
$n_\perp$	refractive index for the perpendicular ray
OD	optical density
$P(\lambda)$	spectral power
Q	response of the detector
Q_{dark}	dark response of the detector
Q_{OFF}	response measured without the filter
$Q_{OFF,\,dark}$	dark response measured without the filter
Q_{ON}	response measured with the filter
$Q_{ON,\,dark}$	dark response measured with the filter
Q_{ref}	response of the reference detector
$Q_{ref,\,dark}$	dark response of the reference detector

$R(\lambda)$	spectral reflectance
s_x	horizontal step size
s_y	vertical step size
$S(\lambda)$	spectral power responsivity of the detector
$S_{ref}(\lambda)$	spectral power responsivity of the reference detector
t	exposure time
$T(\lambda)$	spectral transmittance
w_0	waist radius of the fundamental TEM_{00} laser beam
W_0	waist radius of the real laser beam
x	horizontal position
$\bar{x}(\lambda)$	CIE 1931 color matching functions
$\bar{y}(\lambda)$	
$\bar{z}(\lambda)$	
X_{CIE}	tristimulus values of CIE 1931 XYZ color space
Y_{CIE}	
Z_{CIE}	
y	vertical position
YI	yellowness index

Abbreviations

AEL	Accessible Emission Limit
CIE	Commission internationale de l'eclairage (International Commission on Illumination)
CVC	Current-to-Voltage Converter
GPIB	General Purpose Interface Bus
HeCd	Helium Cadmium
HeNe	Helium Neon
IEC	International Electrotechnical Commission
IEEE-488	GPIB connection standard
IR	Infrared
$KrAr^+$	Krypton Argon Ion
LASER	Light Amplification by Stimulated Emission of Radiation
LIA	Laser Institute of America
LPC	Laser Power Controller
M	Mirror
MgO	Magnesium Oxide

MIKES	Mittatekniikan keskus (Centre for Metrology and Accreditation)
MRI	Metrology Research Institute (MIKES-Aalto Mittaustekniikka)
MUX	Multiplexer
N-BK7	Borosilicate Glass
ND	Neutral Density
OAP	Off-Axis Parabolic Mirror
PQED	Predictable Quantum Efficient Detector
PS	Polystyrene
RS-232	Serial connection standard
Si	Silicon
SP	Technical Research Institute of Sweden
STUK	Säteilyturvakeskus (Radiation and Nuclear Safety Authority Finland)
TEM	Transverse Electromagnetic Mode
TEM_{00}	Fundamental Transverse Electromagnetic Mode
TUT	Tampere University of Technology
USB	Universal Serial Bus
UV	Ultraviolet
UVIADEM	UV Radiation Induced and Assisted Degradation of Materials
Xe	Xenon
XYZ	XYZ color space defined by CIE in 1931

1 Introduction

Optical detectors are used in various applications ranging from imaging devices, security systems, and robotic vision, to signaling and transmission systems. Spectral power responsivity and spatial uniformity are crucial parameters for characterizing detectors. Usually these measurements are carried out, either with a narrow laser beam, or with a focused beam produced by a lamp-based monochromator. Spatial uniformity requires measurements across the active area of the detector. As compared to a monochromator, a laser-based measurement setup has a relatively simple structure, known fixed wavelengths, wide power range, polarization purity, and a small beam diameter. Lasers also have long life-times unlike lamps used with monochromators. In addition, since the laser beam is highly directional, the power level of the beam can be stabilized with an intensity stabilizer. A similar measurement setup can also be used to characterize optical properties of materials.

A laser-based measurement setup with a stabilized, polarized and collimated laser beam is ideal for characterizing, e.g., novel PQED (Predictable Quantum Efficient Detector) detectors [1] developed at Aalto University and MIKES (Centre for Metrology and Accreditation). The spectral responsivity of the PQED is fundamentally known, which can be verified with comparisons.

Polystyrene (PS) and many other materials degrade by turning yellow when exposed to ultraviolet (UV) radiation. This photoyellowing can be quantified with yellowness indices derived from the transmittance or the reflectance spectrum of the material [2]. All photodegradation mechanisms including photoyellowing are functions of the exposure wavelength often described with an action spectrum [3]. Previously, Heikkilä *et al.* have measured the UV action spectrum of regular newsprint photoyellowing with a colorimeter [4]. One of the problems noted was the relatively large measurement beam of the colorimeter used causing convolution, i.e., averaging of color over large exposure wavelength range.

In this thesis, a multi-wavelength setup based on lasers is developed for characterizing optical detectors and materials. The setup directs a stable, collimated laser beam with a narrow beam diameter to a sample plane mounted on a high-resolution XY translation stage. With the measurement setup, the spatial uniformities of two different types of optical detectors were scanned and the absolute power responsivity of one detector was calibrated. To demonstrate how to quantify properties of transparent materials with the measurement setup, polystyrene samples were first exposed to spectrally dispersed UV radiation using a spectrograph [5, 6]

and then measured with the setup. With the setup developed, spectral convolution in the transmittance data is minimal due to the sharp laser beams.

The content of this thesis is arranged as follows. Chapter 2 presents the design and construction of the multi-wavelength measurement setup based on lasers. The measurement setup is automated and controlled with the LabVIEW software described in Chapter 3. Characteristics related to the quality of the laser beams of the measurement setup, such as the beam stability and profile, have been determined in Chapter 4. Chapter 5 presents results of different application measurements, characterization of two different types of optical detectors, and scanning the transmittances of UV degraded polystyrene samples, carried out with the measurement setup. Chapter 6 introduces safety related laser regulations [7, 8, 9, 10], and how they have been taken into account in the setup. Finally, the thesis is concluded in Chapter 7.

2 Measurement setup

The structure of the optical measurement setup designed and constructed in this thesis is presented in Figure 1. Three lasers (Light Amplification by the Stimulated Emission of Radiation) [11] with different wavelengths are used as light sources. The lasers are krypton argon ion laser ($KrAr^+$) with nine wavelengths from 476 nm to 676 nm, helium neon laser (HeNe) with a wavelength of 633 nm, and infrared diode laser (IR diode) with a wavelength of 940 nm. The use of multiple laser wavelengths enables characterizing optical detectors and materials over a wide spectral range.

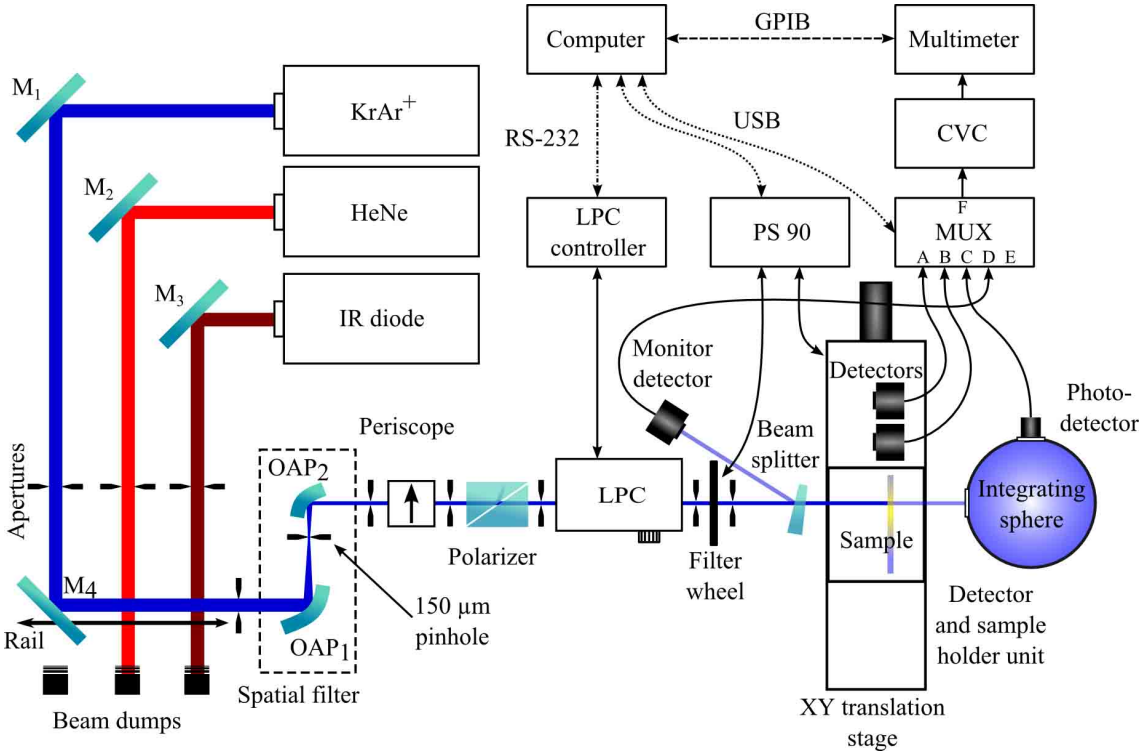

Figure 1: Structure of the multi-wavelength measurement setup based on lasers. Symbols M and OAP indicate a plane mirror and an off-axis parabolic mirror. LPC, MUX and CVC indicate a laser power controller, a multiplexer and a current-to-voltage converter. PS 90 controls a motorized XY translation stage and a filter wheel.

The measurement setup has been designed so that the lasers installed can all be on simultaneously. The laser beams are directed towards an optical rail using plane mirrors M_1–M_3 and the beam is selected by sliding a plane mirror M_4. The unused beams are absorbed by beam dumps, which are used in the setup for safety. A similar mirror-based selector is previously introduced by Hoyt *et al.* [12]. The

selected beam travels through a spatial filter constructed from two off-axis parabolic mirrors (OAP_1, OAP_2) and a pinhole located in the common focal point between the mirrors. The spatial filter produces a smooth beam profile with Gaussian intensity distribution reducing uncertainty of the measurements. The height of the beam is adjusted with a periscope. Since the spatial filter together with a temperature dependent spatial drift of the laser beam may cause long-term drift in the beam power, a laser power controller (LPC) is used to stabilize the beam. The LPC used requires vertically polarized light, and thus a polarizer is mounted in front of its entrance. After the LPC, the power level can temporarily be dropped or blocked with a filter or a baffle assembled in a filter wheel. A detector and sample holder unit is located on a motorized XY translation stage. The measurement setup provides an option to monitor the power level of the laser beam as a reference that can be used to compensate the remaining fluctuations of the stabilized beam power. This is implemented by reflecting a fraction of the stabilized beam back to a monitor detector with a wedged plate beam splitter.

The lasers installed and available for the setup are presented in Table 3. HeCd stands for helium cadmium. The characteristics presented determine the beam quality of each laser. For example, a beam quality factor M^2 describes how much the beam profile resembles a Gaussian intensity distribution of fundamental transverse electromagnetic mode (TEM_{00}). The M^2 value of 1 indicates a pure TEM_{00}. For a multi-mode laser, the M^2 value significantly deviates from 1 since the beam contains higher order transverse electromagnetic modes (TEM). For a highly diverging beam, the beam diameter expands as a function of the distance. Polarization of the beam depicts how the electromagnetic waves of light are oscillating.

Table 3: Characteristics of the lasers installed and available for the setup specified by manufacturers.

Laser type	Manufacturer Model	λ nm	Transverse mode	Polarization	P_{min} mW	P_{max} mW	Diameter [a] mm, %		Divergence mrad, %		M^2
$KrAr^+$	Melles Griot 35-KAP-431	476	TEM_{00}	Linear	4	250	0.7	±2.5	1.0	±5	1.3
		483			10		0.7		1.0		1.2
		488			20		0.7		1.0		1.2
		496			4		0.7		1.0		1.2
		514			10		0.7		1.0		1.2
		520			20		0.7		1.0		1.1
		568			20		0.8		1.1		1.1
		647			20		0.8		1.1		1.1
		676			6		0.8		1.1		1.1
HeNe	Thorlabs HRP005S	633	TEM_{00}	Linear	0.5	2	0.57	–	1.41	±7	<1.1
IR diode	Power Technology Inc. IQ6	940	TEM_{00}	Linear	90	90	>1.0	–	<1.0	–	<1.2
HeCd [b]	Kimmon Koha IK5551R-F	325	TEM_{00}	Linear	15	15	1.1	–	<0.5	–	–
		442			60	60	1.2				
HeCd [c]	Melles Griot 2056-M-A02	325	Multi-mode	Linear	10	10	2.0	–	2.9	–	14.0
		442			30	30	1.9				9.0
IR HeNe [c]	Melles Griot 25-LIP-151-230	1523	TEM_{00}	Linear	0.6	0.6	1.26	–	1.59	–	<1.05

[a] $1/e^2$ from the intensity maximum
[b] Will be ordered
[c] Not currently installed

The setup can be used for various measurements, such as absolute power calibration of optical detectors and transmittance measurements of transparent materials. The absolute power of a detector is calibrated by comparing a response of the detector to a reference detector. In the transmittance measurements, the transmitted beam is collected with an integrating sphere and measured with a photodetector as illustrated in Figure 1. When the measurement setup is used to measure photodiode-based detectors with the current output, the current is converted to voltage to keep the detector in the linear region also known as the photoconductive mode. This is achieved by using a current-to-voltage converter with small input resistance that does not interfere with the current during the measurement. A multiplexer is used in the setup for taking all the measurement readings with one multimeter. The setup is automated, and it can be controlled from a computer using the LabVIEW software which is described in more detail in Chapter 3.

2.1 Laser beam selection and alignment

In the measurement setup, the mirrors used to redirect the laser beams have to be usable over a wavelength range of 200–1600 nm in order to reflect all the laser wavelengths available presented in Table 3. Figure 2 shows spectral reflectances $R(\lambda)$ of silver and aluminium mirrors (Thorlabs PF10-03-P01, PF10-03-F01). Silver mirrors have higher and more consistent reflectance throughout the visible wavelength region as compared to aluminium mirrors. Aluminium mirrors of Thorlabs are UV enhanced, and thus better below 400 nm.

The mirrors M_1–M_3, used to redirect the beams of the lasers installed towards a 300-mm long optical rail, are made of silver. The moveable mirror M_4 for selecting the beam, as well as all the subsequent mirrors used in the spatial filter and in the periscope, is made of UV enhanced aluminium allowing to use UV lasers as the light sources in the measurement setup.

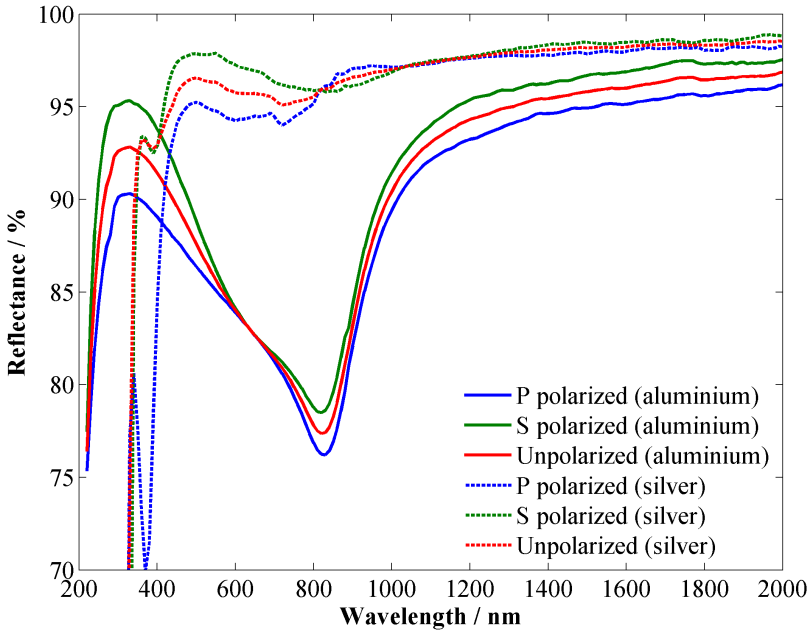

Figure 2: Spectral reflectances of silver and aluminium mirrors (Thorlabs PF10-03-P01, PF10-03-F01).

With my mirror-based beam selector the wider wavelength range of 200–1600 nm is achieved as compared to the wavelength range of 400–700 nm of conventional technique based on visible range cubic beam splitters made of Borosilicate glass (N-BK7) [13, 14]. In addition, the power level is not dropped needlessly in my measurement setup that would be the case when mounting several cubic beam

splitters one after the other. Moreover, my mirror-based approach does not suffer from the ghost reflections, which would cause interference creating undesirable fluctuations in the beam power.

2.2 Beam shaping

Lasers are used as the light sources in my measurement setup since they produce highly monochromatic, coherent and directional light. Photons of the coherent light travel in phase in space and time. Coherence is typically divided to a temporal coherence, which is a measure of the monochromaticity of the light, and a spatial coherence, which is a measure of the uniformity of phase across the optical wavefront. Monochromaticity and coherence together with the geometry of the laser cavity creates a highly directional beam with minimum angular spread. No other light sources have such characteristics. [11]

Figure 3 illustrates how an external laser beam is formed with a mirror-based laser cavity. The beam waist w_0 is defined as the cross-sectional radius where the wavefront of the laser beam is flat. The external laser beam diverges at an angle of θ, thus expanding the beam diameter as a function of the distance. The diameter of the external laser beam d is defined as the full width at $1/e^2 \approx 0.1353$ of the intensity maximum of the beam profile.

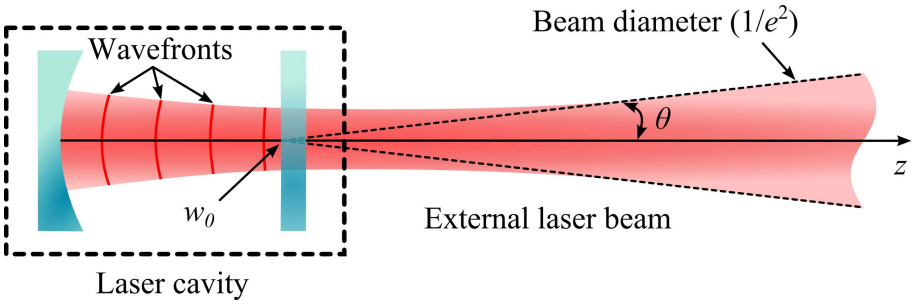

Figure 3: Internal and external beams for a mirror-based laser cavity (redrawn) [15].

For a fundamental transverse mode (TEM_{00}) laser with Gaussian intensity distribution, the divergence angle θ is directly proportional to the wavelength λ and inversely proportional to the beam waist radius w_0 according to [15]

$$\theta = \frac{\lambda}{\pi w_0} . \tag{1}$$

However, no real laser produces pure TEM_{00} transverse mode. Since such lasers do not exist, a beam quality factor M^2 is added to equation (1) resulting in

$$\Theta = \frac{M^2 \lambda}{\pi W_0}\,, \tag{2}$$

where Θ is the divergence angle and W_0 is the beam waist radius of the real laser beam.

Although lasers produce highly monochromatic, coherent and directional light, their beam profiles may contain the higher order transverse modes that require filtering. To improve the profiles of the laser beams used in the measurement setup, an optical spatial filter is used to filter out the higher order transverse modes resulting in the beam profile with Gaussian intensity distribution. Typically, a spatial filter is constructed from two plano-convex lenses and a pinhole located in the common focal point between the lenses. However, in my setup the focal lengths f of the lenses would change due to the varying wavelengths of the lasers causing chromatic aberration. It could be compensated at a certain wavelength range, e.g., 400–700 nm by using achromatic designs, such as achromatic doublet or triplet lenses [11, 16]. However, the chromatic aberration can be eliminated completely by replacing the plano-convex lenses with off-axis parabolic mirrors as used, e.g., by Minoni *et al.* [17].

In addition to the chromatic aberration, various other aberrations exist in optics. For example, all lenses and mirrors with rounded surface have spherical aberration which can be compensated either by improving the manufacturing process or by using deformable mirrors [16]. Off-axial aberration also called coma can be eliminated completely by aligning the beam perpendicularly to pass through the center of the lens or the mirror [11].

I selected a reflectance-based configuration for the spatial filter of my measurement setup to achieve wavelength independency over a wide spectral range of 200–1600 µm. A photograph of this spatial filter is shown in Figure 4. It has been constructed from two off-axis parabolic mirrors (Thorlabs MPD254508-90-F01, MPD127254-90-F01) and a pinhole located in the common focal point between the mirrors. The collecting mirror has a reflective f of 10.16 cm, and the collimating mirror has a reflective f of 5.08 cm. This configuration reduces the beam diameter approximately two times smaller depending on the beam quality factor M^2, but at the same time the beam divergence is increased as stated in equation (2). Both parabolic mirrors have an off-axis angle of 90°. The diameter of the pinhole (Thorlabs P150S) was empirically selected to be 150 µm.

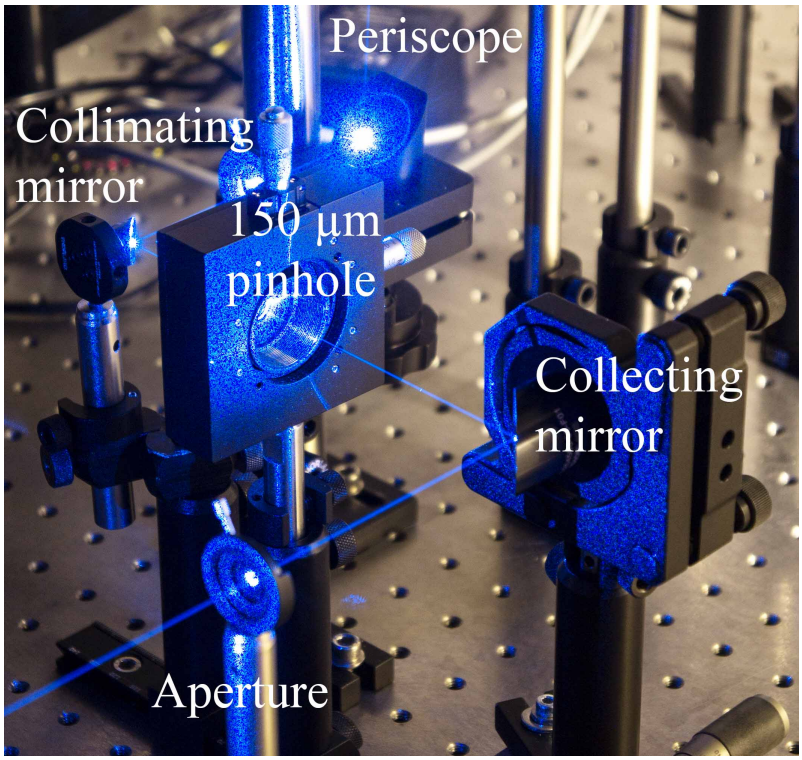

Figure 4: Spatial filter consisting of two off-axis parabolic mirrors (left and right) and a 150 µm pinhole (center).

To ensure the quality of the beam, a beam profiler (Thorlabs BP209-VIS/M) [18] was included in the setup. The profiler was selected to the setup since its UV-enhanced silicon (Si) photodiode-based detector provides a wide wavelength range of 200–1100 nm. The profiler allows measuring of laser beams with diameters from 2.5 µm to 9 mm. Depending on the slit size, the profiler can measure spectral power of 10 nW – 10 W. A smaller slit size enables more accurate low power measurements. In addition to the beam profile measurements, the profiler is a helpful tool, e.g., for aligning the laser beam through the pinhole of the spatial filter due to its fast response and clear measurement software.

2.3 Adjusting beam power

The power of a laser beam fluctuates as a function of the ambient temperature. In addition, the changing ambient temperature increases spatial drift of the laser beam. The spatial filter used in the measurement setup together with spatial drift of the laser beam may increase the power fluctuations. Therefore, a laser power controller (BEOC LPC-VIS) [19] has been installed after the spatial filter in the

measurement setup to stabilize the beam power to a desired level.

Figure 5(a) shows an image of the LPC. It consists of an optical feedback module and a separate electrical module. This LPC was selected to the setup as it operates at a power range of 0–4 W at wavelengths of 425–780 nm. The wavelength range can be extended with special remote detectors. According to the manufacturer, the LPC is able to stabilize the beam outside the reported wavelength range with a loss of the power level reliability. The LPC requires collimated, vertically polarized, either continuous or chopped beam with a chopping frequency over 100 kHz.

The operating principle of the optical feedback module is illustrated in Figure 5(b). A fraction of the incoming beam is reflected by a beam splitter and measured with a photodiode. The amplified difference between the measured signal and the reference signal adjusts a modulator to maintain the beam power. The photodiode is temperature controlled, and thus changes in the ambient temperature do not cause error in the control. The beam stabilizer can be controlled through the front panel of the electrical module shown in Figure 5(a) or via RS-232 interface.

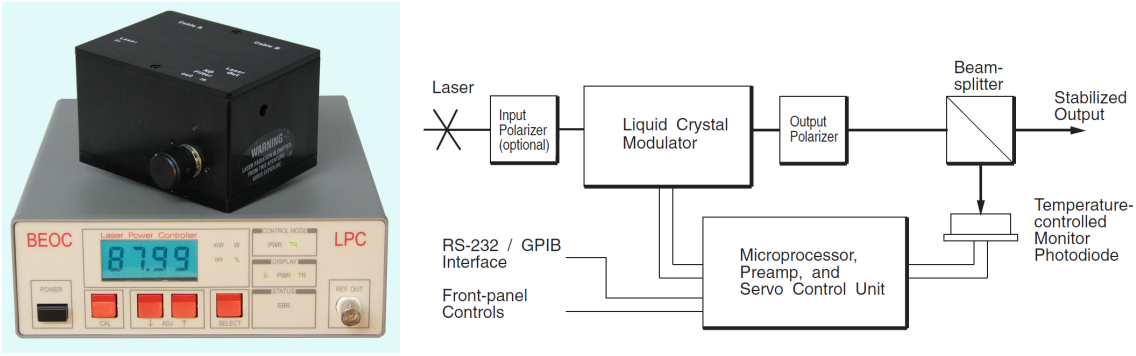

(a) **(b)**

Figure 5: Laser power controller (BEOC LPC-VIS) consists of an electronic controller module and an optical feedback module. Figure shows (a) the modules and (b) the operating principle of the optical feedback module. [19]

The laser power controller requires vertically polarized light to be able to control the signal properly. A Glan-Thompson calcite crystal polarizer (Thorlabs GTH10M) with the extinction ratio of 10^5:1 and the field of view angle of 40° is used in this setup. It is built out of two prisms combined with their long faces as illustrated in Figure 6. The polarizer is based on the birefringence of calcite as the unpolarized light experiences double refraction. Therefore, the first prism separates the unpolarized light into two polarized rays at different angles. For example, if the wavelength of the incident laser beam is $\lambda = 589.3$ nm, the refractive index for the

parallel ray is $n_{\parallel} = 1.486$ and $n_{\perp} = 1.658$ for the perpendicular ray. Depending on the orientation of the polarizer, one of the rays is reflected at the junction of the prisms. The second prism reorients the propagating ray parallel to the incident unpolarized ray. [11] Using orientation illustrated in Figure 6, the vertically (P) polarized light will travel straight through the crystal, while the horizontally (S) polarized light will exit the crystal at an angle that depends on the wavelength and the length of the crystal.

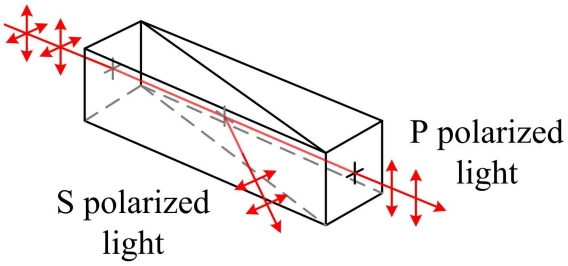

Figure 6: A Glan-Thompson polarizer (Thorlabs GTH10M) separates the incident laser beam into the vertically (P) and horizontally (S) polarized beams.

After the LPC, the power level needs to be varied temporarily when comparing different types of detectors. For example, photodiode-based detectors saturate with beam power over 1 mW [20]. Therefore, a motorized filter wheel (OWIS FRM 40-6-D25-HiDS) with six filter holders is added to the measurement setup. One holder has been left empty and another holder blocks the beam with a baffle acting as a beam shutter. The shutter is needed in the setup as the effect of stray light and offset of the measurement electronics have to be corrected from the response when measuring with a detector. Neutral density (ND) filters with nominal transmittance values of 1 % and 10 % were mounted in the four remaining holders. Two of them are absorptive (Thorlabs NE10B, NE20B) and the other two are reflective (Thorlabs NDUV10B, NDUV20B). The transmittance spectra of the filters are shown in Figure 7.

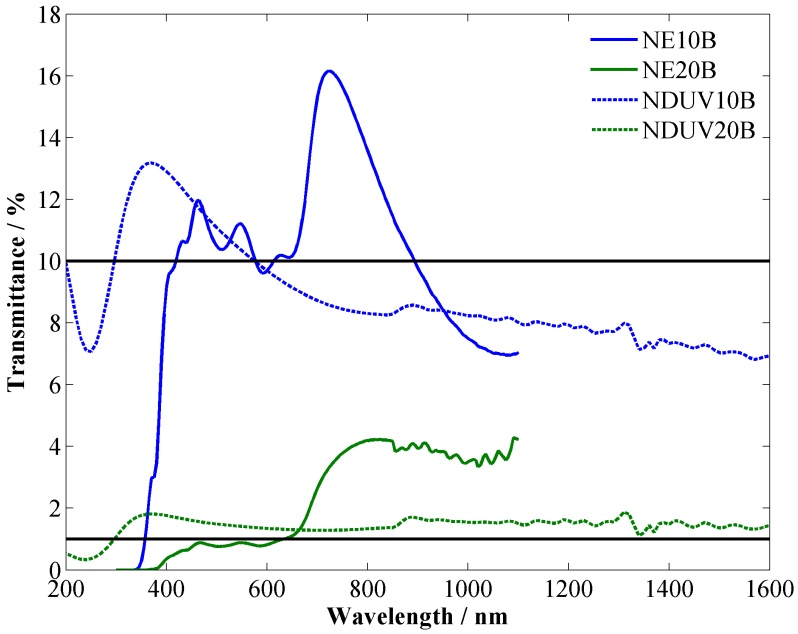

Figure 7: Spectral transmittances of neutral density filters of Thorlabs.

2.4 Detector and sample holder unit

The detector and sample holder unit is located on the motorized XY translation stage (OWIS LIMES-150-DS130, LIMES-150-DS220). The XY translation stage has a resolution of 0.1 µm and accuracy of ±0.3 µm/m allowing scanning detectors and samples spatially with high resolution. This section describes how the measurements are carried out.

2.4.1 Measuring properties of detectors

Optical detectors produce typically a current or a voltage signal when their photosensitive area is illuminated with light. For photodiode-based detectors, the corresponding responsivity (A / W) [21] is

$$S(\lambda) = \frac{i(\lambda)}{P(\lambda)}\,, \tag{3}$$

where $i(\lambda)$ is the photocurrent, and $P(\lambda)$ is the optical input power at the laser wavelength of λ. When measuring the responsivity of a detector, the detector is aligned by adjusting the screws of the holder until the laser beam hits perpendicularly to its center according to Figure 8.

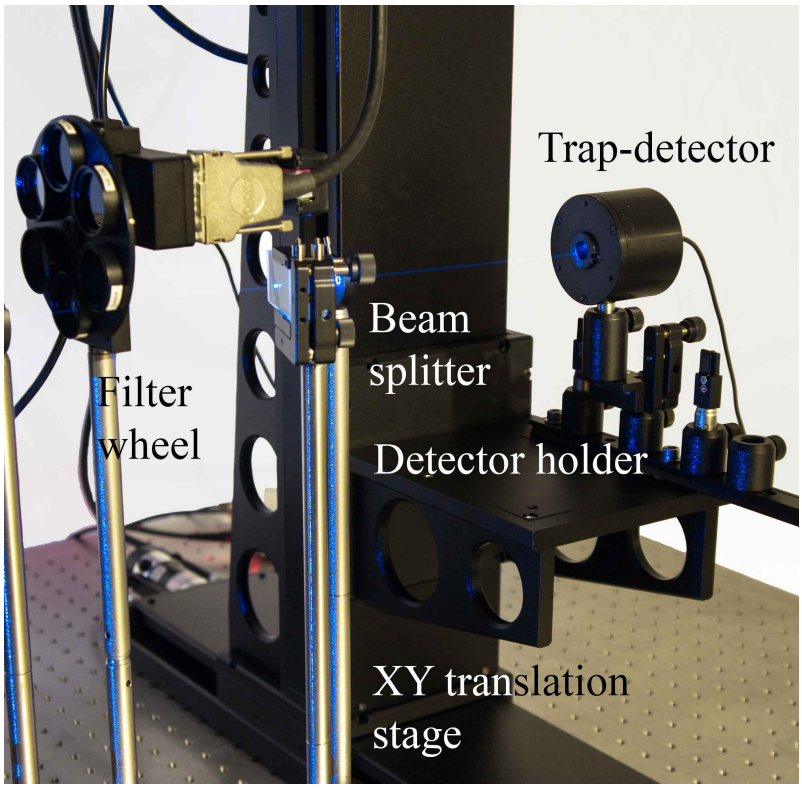

Figure 8: A trap detector being measured.

The absolute power responsivity $S(\lambda)$ of a detector can be calibrated against a reference detector traceable to primary reference standard as

$$S(\lambda) = \frac{Q(\lambda) - Q_{dark}(\lambda)}{Q_{ref}(\lambda) - Q_{ref,\,dark}(\lambda)} S_{ref}(\lambda)\,, \tag{4}$$

where the $Q(\lambda)$ and $Q_{ref}(\lambda)$ are the responses of the detector and the reference detector. $S_{ref}(\lambda)$ is the responsivity of the reference detector. The dark responses $Q_{dark}(\lambda)$ and $Q_{ref,\,dark}(\lambda)$ are also measured and corrected from the responses.

During the calibration, a detector and a reference detector are measured one at a time. Measurement is repeated several times to improve the uncertainty of the calibration by minimizing the standard deviation of the mean

$$\sigma_M = \frac{\sigma}{\sqrt{n}}\,, \tag{5}$$

where σ is the standard deviation and n is the sample size.

Four detectors can be installed simultaneously on the detector holder unit allowing simultaneous calibration of three detectors. The detectors can be connected to the multiplexer (Signal Recovery 3830 multiplexer) input ports A–E. The port F

is set as the output of the multiplexer.

In addition to the calibration of the absolute power, a spatial uniformity of a detector can be scanned with the setup. The spatial uniformity reveals the condition of a detector. For example, dust particles can be seen as a drop in the uniformity. The beam diameter used in the calibration affects the responsivity of a detector, and thus it has to be recorded in the calibration certificate. The responsivity of a calibrated detector can be corrected for beam diameter with the spatial non-uniformity data, when measuring with the different beam diameter as compared to the calibration.

When calibrating detectors at high power levels, the response of some detector types may saturate after a certain power level. In this sort of situation, the power level can be decreased with the neutral density filters introduced in Chapter 2.3. The filters have to be calibrated each time when calibrating a detector as their transmittance properties may change over time. Since their transmittance spectra are not flat as can be seen in Figure 7, the calibration is valid only for one wavelength. The transmittance of a filter is measured as

$$T(\lambda) = \frac{Q_{ON}(\lambda) - Q_{ON,\,dark}(\lambda)}{Q_{OFF}(\lambda) - Q_{OFF,\,dark}(\lambda)}\,, \tag{6}$$

where Q_{ON} and Q_{OFF} are the responses measured with and without the filter. $Q_{ON,\,dark}$ and $Q_{OFF,\,dark}$ are the corresponding dark responses.

2.4.2 Measuring properties of materials

This setup can be used widely to characterize various optical properties of materials by scanning their transmittances. A material sample being measured is attached to the detector and sample holder unit perpendicularly to the laser beam according to Figure 9. The transmitted laser beam is collected with the integrating sphere and measured with the photodetector.

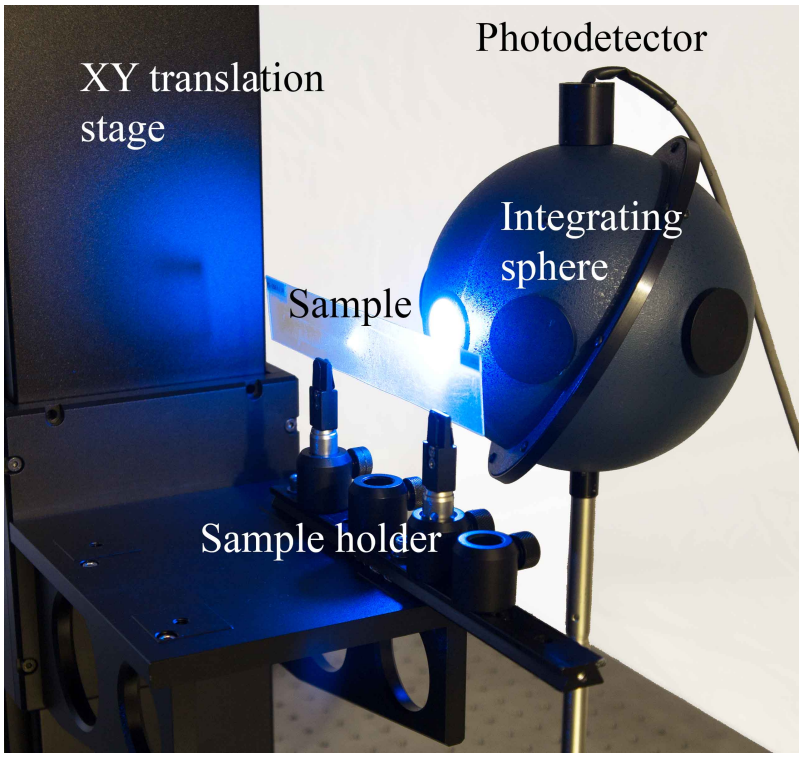

Figure 9: A polystyrene sample being measured.

Here, we use this setup to measure the yellowness index of UV degraded polystyrene samples. The samples were degraded by exposing them to spectrally dispersed UV radiation for different time periods using a spectrograph developed by Kärhä *et al.* [5, 6]. The transmittances of the samples at various measurement wavelengths were then scanned with the measurement setup. Spatial scan with high resolution gives transmittances at regions exposed to different UV wavelengths that can be used to derive the action spectrum of polystyrene photoyellowing using a yellowness index.

Yellowness index stands for magnitude of yellowness relative (%) to magnesium oxide (MgO) measured under natural daylight, and it can be calculated from the color coordinates according to [2]

$$YI = \frac{100(1.28X_{CIE} - 1.06Z_{CIE})}{Y_{CIE}} \,. \tag{7}$$

Positive yellowness index indicates substance is yellowish, equal to 0 indicates it is white, and negative indicates it is bluish. The tristimulus values X_{CIE}, Y_{CIE} and Z_{CIE} needed for quantifying yellowness under certain illumination condition $I(\lambda)$ are calculated using CIE 1931 color matching functions (International Commission

on Illumination) [22, 23] $\overline{x}(\lambda)$, $\overline{y}(\lambda)$, $\overline{z}(\lambda)$, and spectral transmittance $T(\lambda)$ as

$$X_{CIE} = \int_{380\text{ nm}}^{780\text{ nm}} I(\lambda)T(\lambda)\overline{x}(\lambda)\mathrm{d}\lambda\,, \tag{8}$$

$$Y_{CIE} = \int_{380\text{ nm}}^{780\text{ nm}} I(\lambda)T(\lambda)\overline{y}(\lambda)\mathrm{d}\lambda\,, \text{ and} \tag{9}$$

$$Z_{CIE} = \int_{380\text{ nm}}^{780\text{ nm}} I(\lambda)T(\lambda)\overline{z}(\lambda)\mathrm{d}\lambda\,. \tag{10}$$

In addition to the yellowness index, various other methods exist for quantifying UV degradation. For example, absorbance can be defined from the measured transmittance as

$$A(\lambda) = \log_{10}\left(\frac{1}{T(\lambda)}\right)\,. \tag{11}$$

Then, concentration c of the material can be derived from the Beer's law [24] as

$$c = \frac{A(\lambda)}{\epsilon(\lambda)l}\,, \tag{12}$$

where the $\epsilon(\lambda)$ is the molar absorption coefficient and l is the thickness of the sample. In optics, absorbance $A(\lambda)$ is known as optical density OD.

3 Software

The setup is controlled with LabVIEW software (LabVIEW 12.0). This chapter introduces the user interface and the main functionalities of the software.

3.1 Technical details

The user interface of the software built for controlling the measurement setup developed is shown in Figure 10.

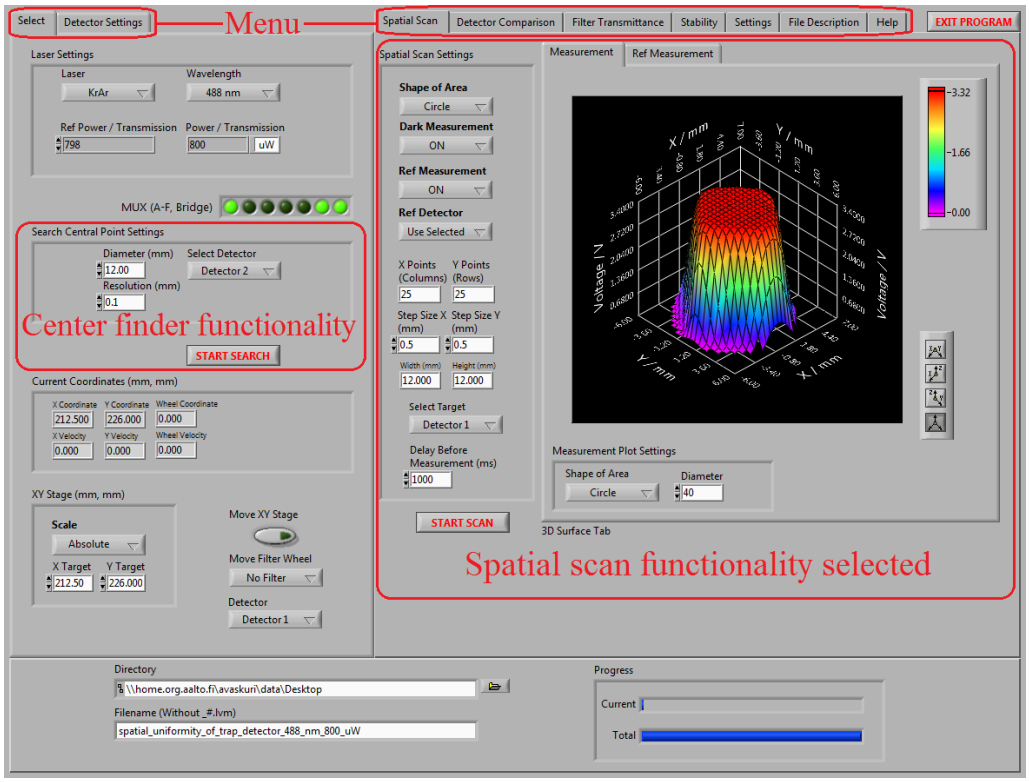

Figure 10: LabVIEW user interface built to control the setup. The red boxes have been added to denote functional blocks of the software. Functionalities other than the Spatial scan shown can be selected in the Menu.

For most devices used in the setup, manufacturers provide ready-made LabVIEW functions. I modified them to work in the software. The XY translation stage and the filter wheel are controlled via USB (Universal Serial Bus) by the control unit (OWIS PS90). Installing the OWISoft, installs also all drivers needed for using LabVIEW. Similarly, LabVIEW drivers for the multiplexer are installed when installing its software. The multiplexer is also connected via USB to the computer. In addition, a ready LabVIEW library exists for the multimeter. The multimeter is controlled

via GPIB (General Purpose Interface Bus, IEEE-488). To communicate with the LPC via serial connection (RS-232), functions were programmed using the standard serial library provided by LabVIEW.

3.2 Implementation of the main functionalities

Various automated functionalities have been added to the software to improve the usability of the measurement setup. Some measurements are time consuming and difficult to carry out without automation, especially those related to spatial scanning.

3.2.1 Center finder

With the automated measurement setup, the detectors are always centered reliably at the same position, and the measurement processes are expedited. If the exact center is known, e.g., a smaller area can be scanned when measuring spatial uniformity of the detector. In addition, the reliability of the absolute power calibrations is improved since the power is typically measured in the center of the detector.

The functionality is implemented as follows. First, the laser beam is directed perpendicularly to the active area of the detector by moving the XY translation stage manually. Then, the detector is scanned horizontally with the desired resolution and diameter throughout its active area. After scanning, the center coordinate of the detector is calculated by finding coordinates where the response is half of the maximum response. The search is started from the outer coordinates with respect to the starting coordinate. Then, the detector is moved to the horizontal center coordinate found. The vertical center coordinate is searched in the same way, and the detector is moved to the vertical coordinate found. The center coordinates of the detector are saved to the corresponding detector settings.

The algorithm has a few limits. The diameter to be scanned should be set roughly 1.5 times larger than the active area of the detector to find the edges of the detector. The algorithm also assumes the active area of the detector is reflection symmetric both vertically and horizontally.

3.2.2 Detector calibration

Implementation of the absolute power calibration functionality introduced in Chapter 2.4.1 is presented in Figure 11. Before measuring, the user sets the reference detector and all detectors to be calibrated. In addition, the user sets the number of

rounds to be measured. Responses of all detectors selected are measured during one round including their dark responses, and all settings and readings are automatically saved to a text file created in the beginning of the calibration.

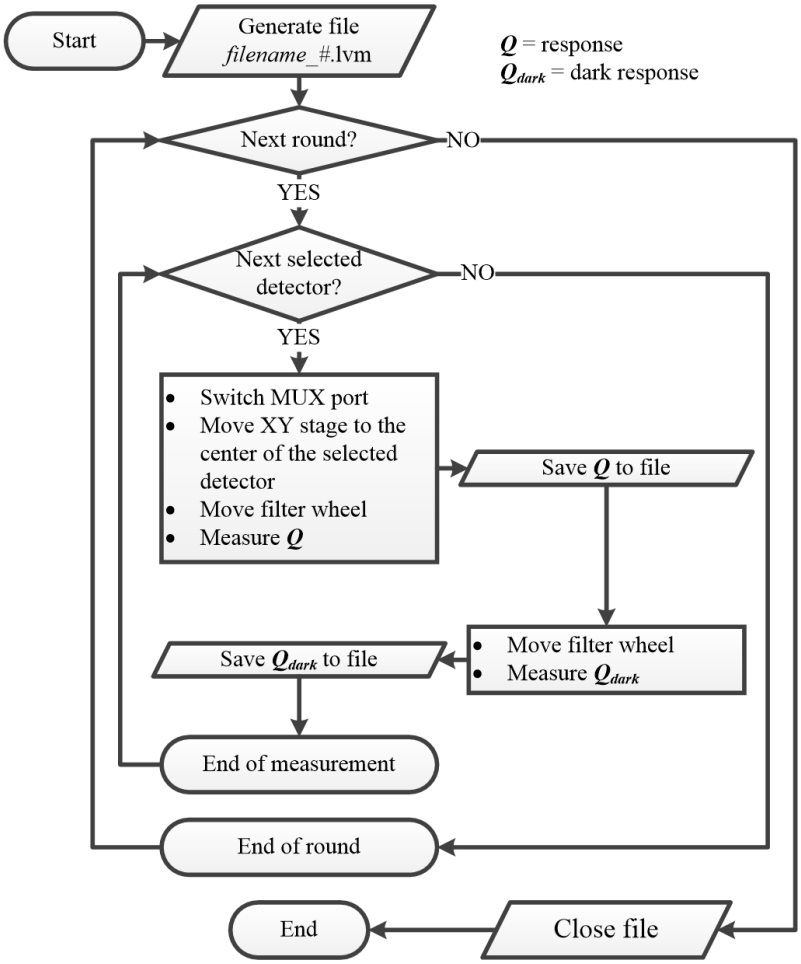

Figure 11: Implementation of the detector calibration functionality.

3.2.3 Filter calibration

Implementation of the filter transmittance measurement functionality introduced in Chapter 2.4.1 is presented in Figure 12. Before measuring, user sets the filter, the detector and the number of rounds to be measured.

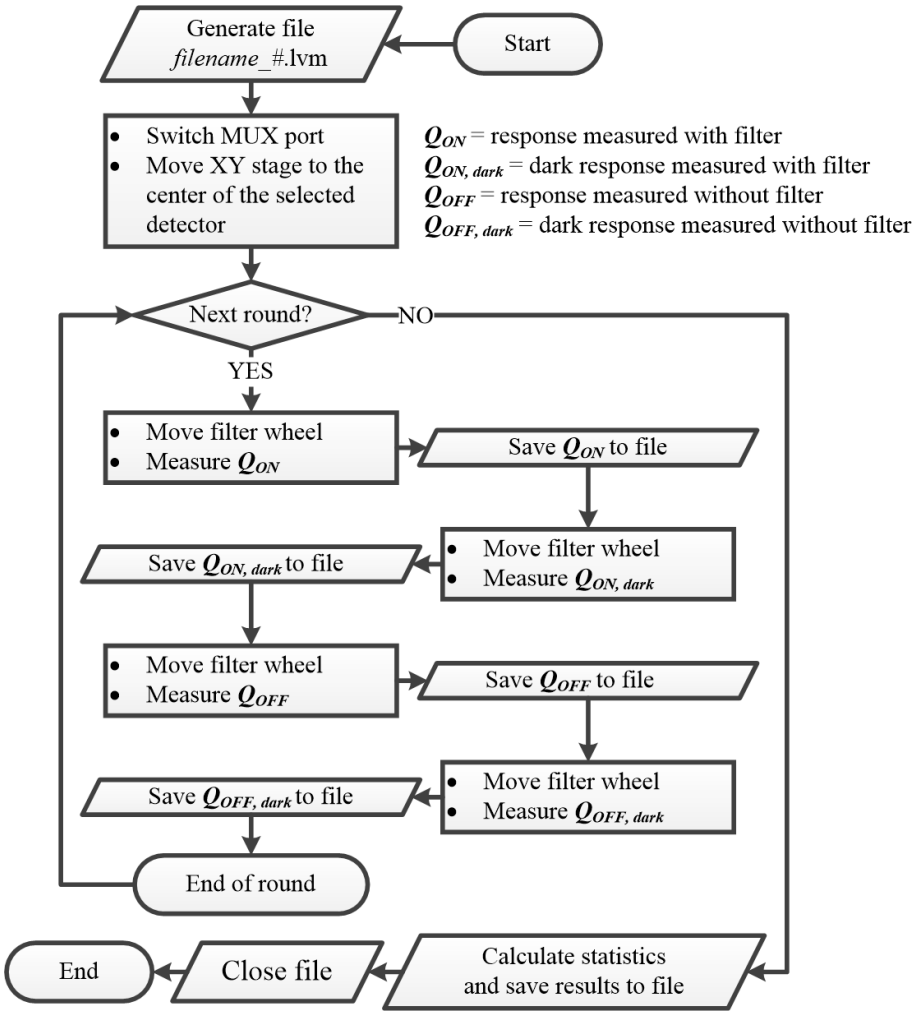

Figure 12: Implementation of the filter transmittance measuring functionality.

3.2.4 Spatial scan

Implementation of the scanning functionality introduced in Chapters 2.4.1 and 2.4.2 is presented in Figure 13. Before scanning a detector, it is recommended to determine its center coordinates with the functionality introduced in Chapter 3.2.1. The scanning functionality contains various elements listed below.

- Select target (Detector 1 / . . . / Detector 4 / Manual)
- Shape of area to be scanned (Rectangle / Circle)
- Number of points (horizontally and vertically separately)
- Resolution (horizontal and vertical separately)
- Dark measurement (ON / OFF)
- Reference measurement (ON / OFF)

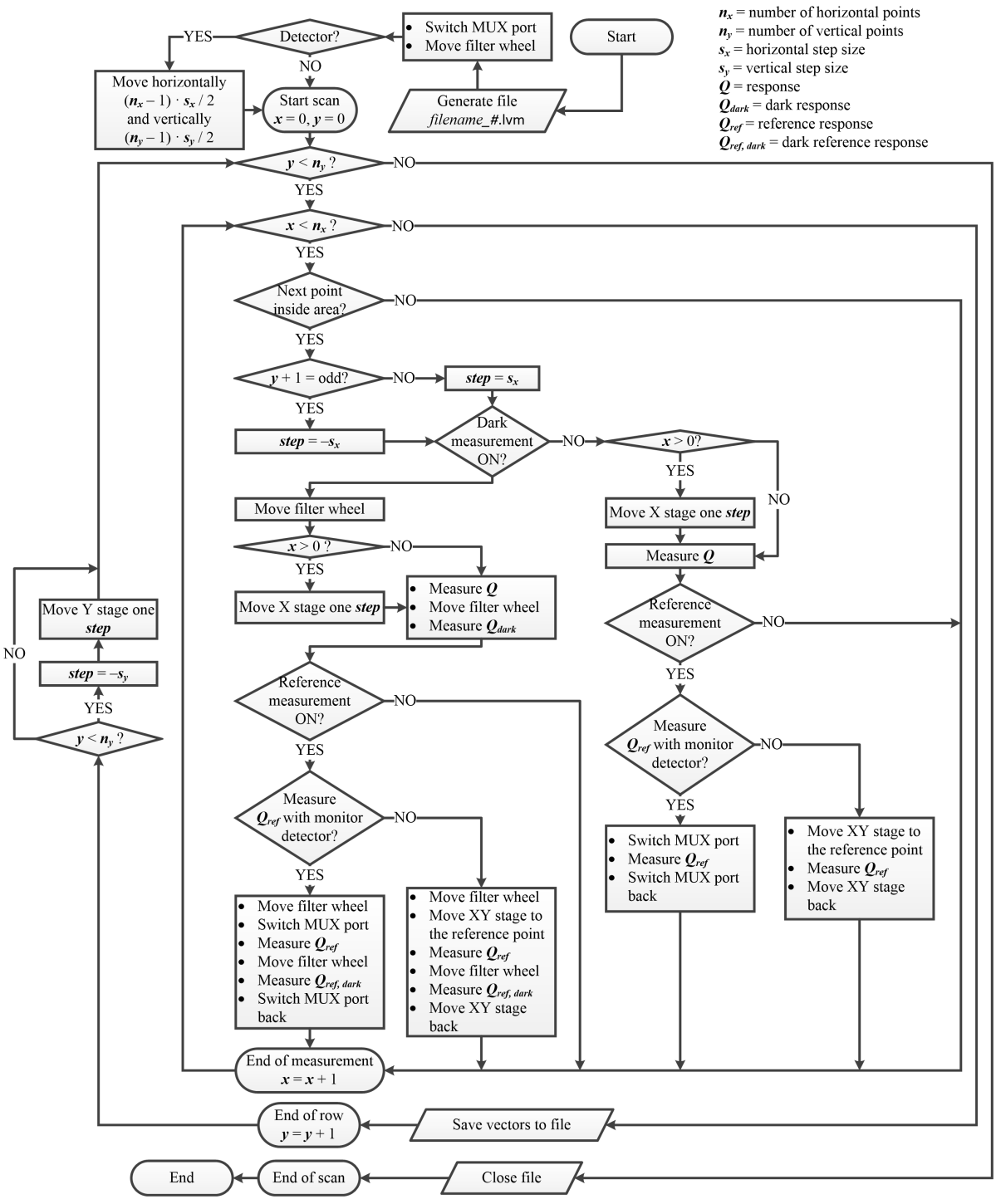

Figure 13: Implementation of the scanning functionality.

The size and the resolution of the area have the largest impact on the total time consumed with the scan. The scan can be slightly expedited by selecting a suitable shape of the area to be the scanned. For example, most detectors have a circle-shaped light sensing area so the corresponding shape is optimal.

Dark measurement can be set ON to correct for the effect of stray light and offset of the measurement electronics as presented in equation (4). In addition, the reference measurement can be set ON to take into account the effect of changes in the detector response due to the fluctuations in the laser power. If the reference measurement is selected, the reference response is always measured after the actual response.

The scan is started in the upper left of the area if the target is set as the detector. If the manual mode is selected, the scan starts from the point where the XY translation stage is at that moment. The odd rows, starting from the first row, are scanned from left to right and the even rows in the opposite direction. Looking at the direction of the incident laser beam, the upper left corner of the XY translation stage is set to (0, 0) and the lower right corner is set to (300, 300). Therefore, the XY translation stage is always transferred to the opposite direction for realizing scanning as described above. Before measuring, the point is checked to fall within the given area. If the point does not lie inside the area, the next point will be checked. After every scanned row, the results are automatically saved to the text file.

4 Performance characterization of the measurement setup

The characterization measurements introduced in this chapter were carried out for verifying the performance of the setup. They quantify the quality of the laser beams, such as the beam profile and the long-term stability of the beam power.

4.1 Beam profile

A spatial filter is used in the setup to improve the quality of the laser beam profile. It was also designed to reduce the beam diameter approximately two times smaller depending on the M^2 value of the laser beam according to equation (2). A narrow laser beam with Gaussian intensity distribution is convenient, e.g., when scanning a spatial surface with a small step size. The narrow beam causes less convolution to the spatial uniformity, thus preserving edges of its deviation sharp.

The effect of the spatial filter used in the measurement setup was tested by measuring the laser beams of $KrAr^+$ laser at the wavelength of 488 nm and IR diode laser at the wavelength of 940 nm before and after the spatial filter shown in Figures 14 and 15. The filtered profile is measured on the detector holder unit. Although the spatial filter reduces the beam diameter, the divergence expands it as a function of the distance. Therefore, the beam diameters of the beam profiles measured on the detector holder unit are not significantly smaller. The spatial filter improves the quality of the laser beam by smoothing the spatial intensity distribution, especially with the diode laser in Figure 15. The gas lasers used (HeNe and $KrAr^+$) already have smooth intensity distribution across their beams. Thus, the spatial filter does not affect significantly their profiles as can be seen in Figure 14.

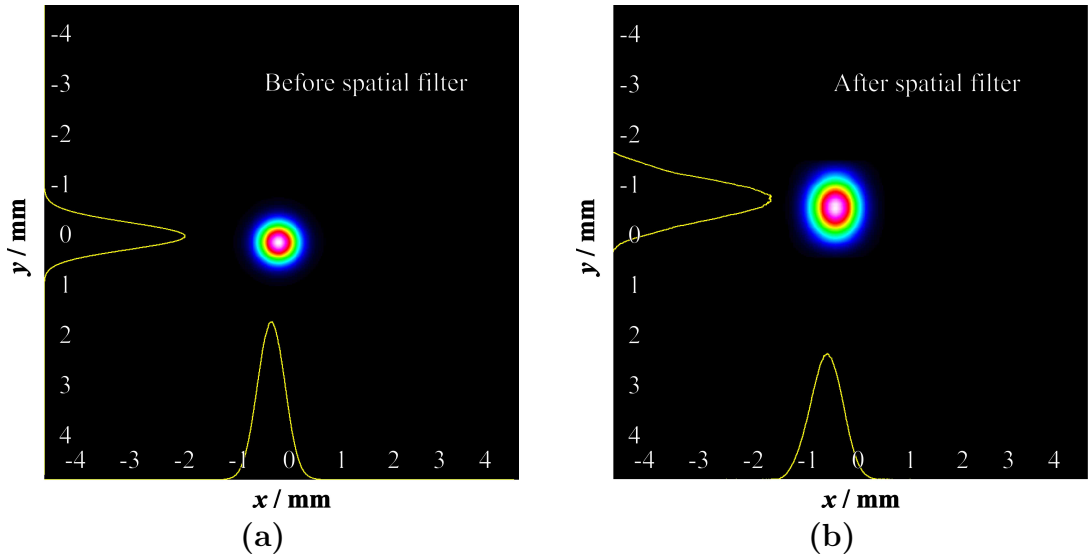

Figure 14: Beam profile of the $KrAr^+$ laser at the wavelength of 488 nm measured (a) before and (b) after the spatial filter. The 2D images have been reconstructed from horizontal and vertical cross sections measured using the Dual Scanning Slit Beam Profiler. The images have been exported from the Thorlabs Beam Software.

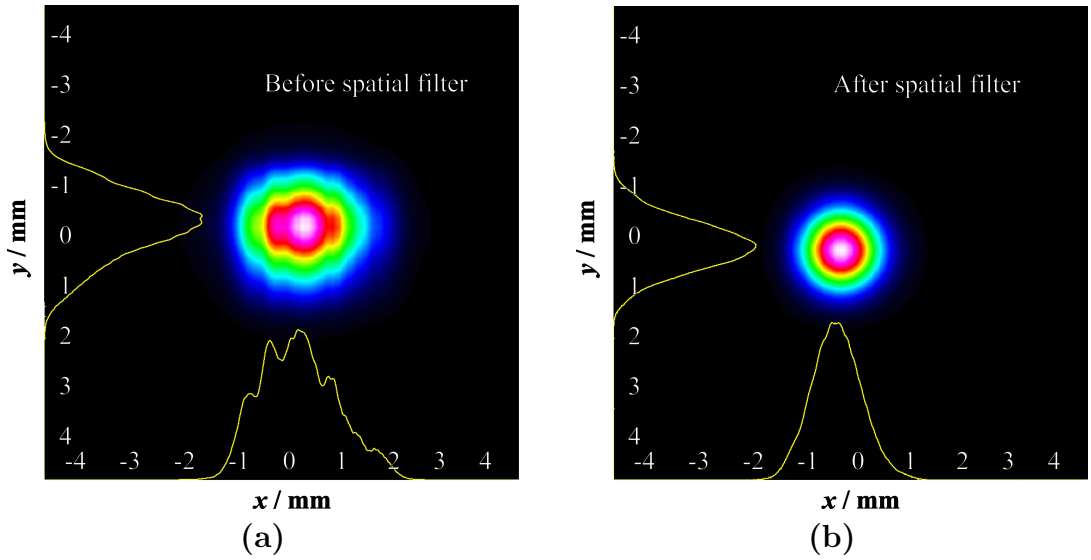

Figure 15: Beam profile of the IR diode laser at the wavelength of 940 nm measured (a) before and (b) after the spatial filter. The 2D images have been reconstructed from horizontal and vertical cross sections measured using the Dual Scanning Slit Beam Profiler. The images have been exported from the Thorlabs Beam Software.

4.2 Long-term stability

Detector calibrations and characterizations may take significant amount of time. During these measurements, it is essential that the laser beam remains stable. The long-term stability of the setup was characterized by measuring one of the laser beams for an 8 h time period with and without the laser power controller. The $KrAr^+$ laser at the wavelength of 488 nm was used as the light source and a 3-element Si-trap detector (UVFR-8) was used as the detector. The laser beam power was measured and registered to a text file at intervals of 20 seconds. The dark response of the trap detector was taken into account by measuring the response of the trap detector while the detector was not illuminated and subtracting it from the actual response. A current-to-voltage converter (Lab Kinetics SP042) was connected between the trap detector and the multimeter with the gain of 10^4 V/A. The DC voltage mode of the multimeter was used. The integration time was set to 100 ms and the sample count was set to 1. The autozero mode was set off, and the manual range of 10 V was used. The same settings of the multimeter and the current-to-voltage converter were used for all stability tests.

Figure 16 shows the long-term stability results. When the stabilization is not used, the response varies slowly about 27 % during a time period of 8 h. When it is used, the power varies within 0.05 % with the relative standard deviation of 0.01 % during the same time period. The use of the laser power controller improves the stability by more than two orders of magnitude. Such a large difference between the stabilities measured is most probably caused by the temperature dependent power and spatial drift of the laser beam together with the spatial filter since the air conditioner cannot completely stabilize the room temperature. Since the pinhole of the spatial filter is stationary, a spatial drift of the beam may change its intensity. Even a small spatial drift in the beginning of the setup can lead to a larger drift further in the setup. For example, the beam position of the $KrAr^+$ laser at the wavelength of 488 nm right before the spatial filter drifts approximately ± 30 µm during a time period of 3 min. Thus, the laser power controller is crucial in the measurement setup.

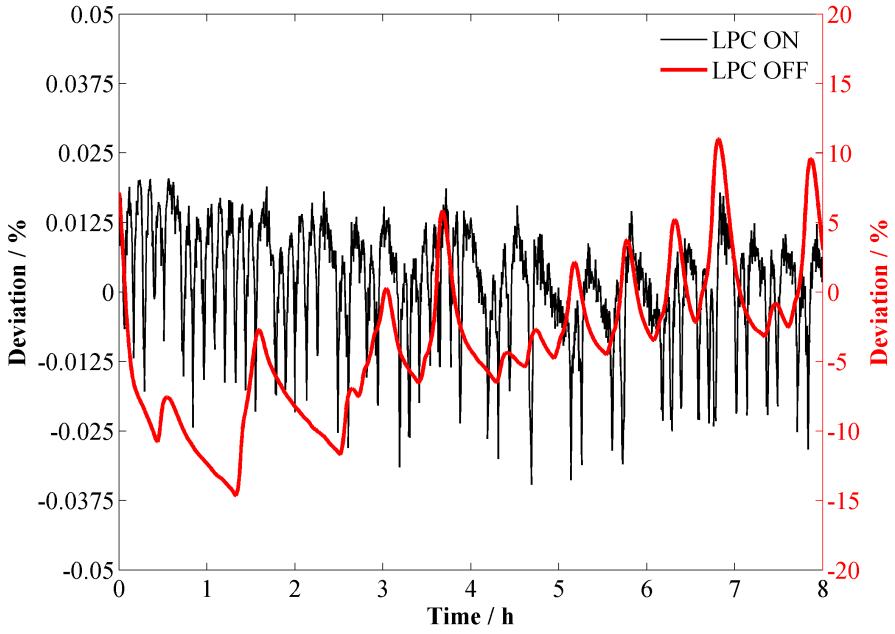

Figure 16: Long-term stability of the measurement setup was determined by measuring the laser beams at the wavelength of 488 nm for 8 h with a 3-element Si-trap detector.

Figure 17 shows a magnified view of the drift within the time period of 3–4 h. As can be seen, there are systematic fluctuations in the stabilized signal, caused by the feedback of the laser power controller. The remaining relative standard deviation of 0.01 % in the stabilized beam was measured to decrease below 0.007 % by taking into account the reference responses of the beam power measured with a monitor detector (UVFR-1).

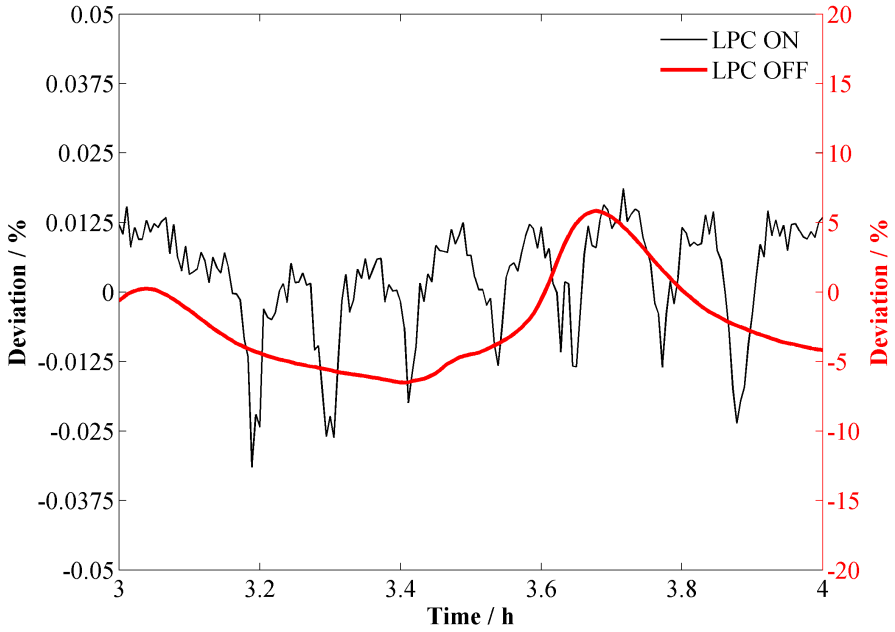

Figure 17: Magnified view of the time period of 3–4 h of the stability measurement.

5 Applications of the measurement setup

Various test measurements were carried out using the setup developed to demonstrate its functions. These include scanning the spatial uniformities of two different types of optical detectors, calibrating the absolute power responsivity of a detector and scanning the spatial transmittances of UV degraded polystyrene (PS) samples.

5.1 Spatial uniformities of optical detectors

Spatial uniformities of two different detectors were measured at several laser wavelengths. The detectors studied were a pyroelectric radiometer (Rk-5720 with detector RkP-575) with two replaceable detector heads labelled as Detector 1 and Detector 2, and a 3-element Si-trap detector labelled as UVFR-8. The spatial uniformity of a detector reveals its quality and condition. For instance, dust particles on the surface of the active area would significantly drop the responsivity of the detector. Spatial uniformity data can also be used to calculate corrections and uncertainties in calibrations and measurements with the detectors.

Test measurements were conducted using the following settings. The detectors were attached to the detector holder unit perpendicularly to the laser beam, as described in Chapter 2.4.1. Then, their centers were determined with the center finder functionality described in Chapter 3.2.1. The trap detector was connected to the multiplexer port A via a current-to-voltage converter (Lab Kinetics SP042). The implementation of the multiplexer was described in Chapter 2.4.1. The gain of the current-to-voltage converter was set to 10^4 V/A. The pyroelectric radiometer has a voltage output that has a sensitivity of 10 V divided by the selected power range (0–200 µW, 0–2 mW, 0–20 mW, 0–200 mW, 0–2 W or 0–20 W). The voltage output of the pyroelectric radiometer was connected directly to the multiplexer port B. The detector outputs after the multiplexer were measured as voltages with a multimeter (Agilent 34401A). The integration time was set to 100 ms, sample count was set to 1 and manual range was set to 10 V.

Detector responsivities vary slowly with time, e.g., due to the fluctuations in the laser power as shown in Figure 16. This was taken into account by measuring the response at a certain reference point between each actual measurement in the scan. In these measurements, the central points of the detectors were used as reference points. The measured spatial response values were divided with the average of the previous and next reference point values to obtain the corrected spatial

uniformity. The spatial uniformity was then scaled to percent, thus corresponding to the deviation of 0 % in the center. The dark measurement was not taken into account in the spatial uniformities except for the trap detector measured at the wavelength of 520 nm. This was because the dark measurement functionality had not been added to the software yet when the measurements were conducted. The spatial uniformities were scanned using a step size of 0.5 mm.

The pyroelectric radiometer consists of two replaceable detector heads, Detector 1 and Detector 2, with circle-shaped active areas of 9 mm in diameter. Both detector heads were scanned at the wavelengths of 488 nm, 633 nm and 940 nm with the beam diameters of 1.0 mm, 1.6 mm, and 1.6 mm, respectively. The spatial uniformities obtained are shown in Figure 18. The spatial uniformities of both detector heads vary approximately 10 % across their active areas. Both detectors have a horizontal junction with higher response. The junction results from the inner structure of the detector. The active area of the pyroelectric detector consists of two pyroelectric elements that are oriented at angles to form a cavity. The first element forms the upper half and the second element forms the lower half of the active area.

As seen in Figure 18, a broader beam size causes more convolution to the response as sharp edges in the spatial response become flattened. The spatial uniformity of the pyroelectric radiometer is quite poor. The detector is used because it is linear over a wide power range upto 10 W, and it is spectrally flat (±0.5 %) over a wavelength range of 250 nm – 16 µm [25].

When the spatial uniformities of Detector 1 and Detector 2 were scanned at the wavelengths of 488 nm and 940 nm using the power of 800 µW, the power range of the pyroelectric radiometer was set to 0–2 mW. When the wavelength of 633 nm with 90 µW was used in the scans, the power range was set to 0–200 µW.

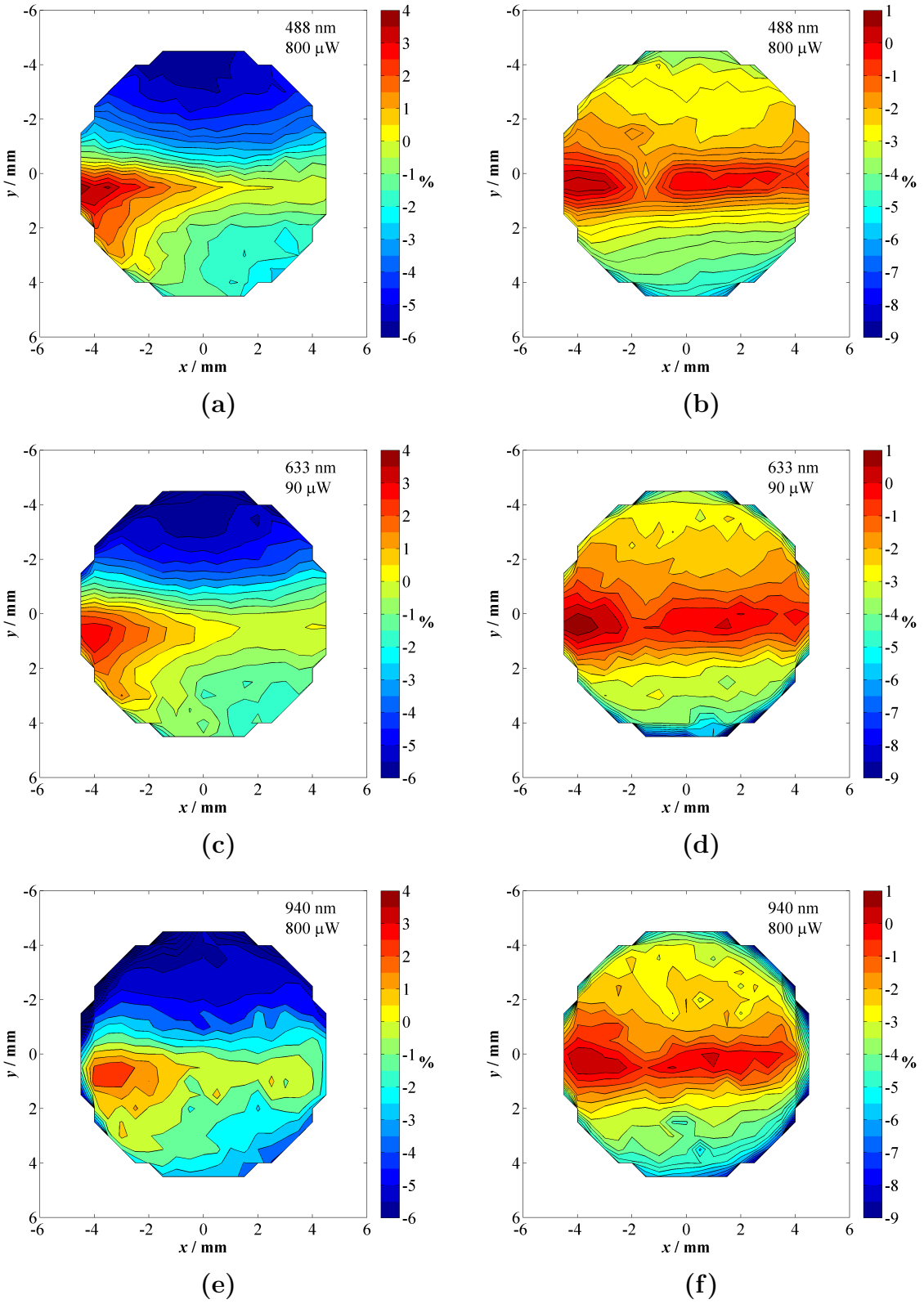

Figure 18: Spatial uniformities of two pyroelectric radiometer heads Detector 1 (on left) and Detector 2 (on right) scanned using a step size of 0.5 mm. The detector heads were scanned at the wavelength of (a)–(b) 488 nm, (c)–(d) 633 nm and (e)–(f) 940 nm.

The studied Si-trap detector is constructed from three photodiodes of type S1337-11 from Hamamatsu. The photodiodes are oriented in a light trapping configuration so that the reflected photons can also be detected. [26]

Figure 19 shows the spatial uniformities of the trap detector measured using $KrAr^+$ laser at the wavelengths of 488 nm, 520 nm and 647 nm with the beam diameters of 1.0 mm, 1.3 mm, and 1.4 mm, respectively. The trap detector has a circle-shaped entrance aperture of 8 mm in diameter, but the active area reminds more of a diamond due to the orientation of the photodiode elements. The usable active area has a diameter of 6 mm.

The spatial uniformities are within 0.1 %, which is a typical variation for aged trap detectors. Spatial uniformities of newly built trap detectors deviate less than 0.03 % [21]. The spatial uniformity of the trap detector about 100 times better than the spatial uniformity measured for the pyroelectric radiometer in Figure 18.

At the times of these measurements, the air conditioner had not been yet installed. Therefore, the ambient temperature rose due to the heat produced by the laser used. The temperature rise in the room increased the response of the reference point as seen in Figure 19(d). In this measurement, the peak-to-peak deviation of the reference point was measured to be 0.05 % affecting significantly the measured spatial uniformity of the trap detector. Thus, in this kind of measurement that demands accuracy higher than 0.05 %, the reference response has to be monitored.

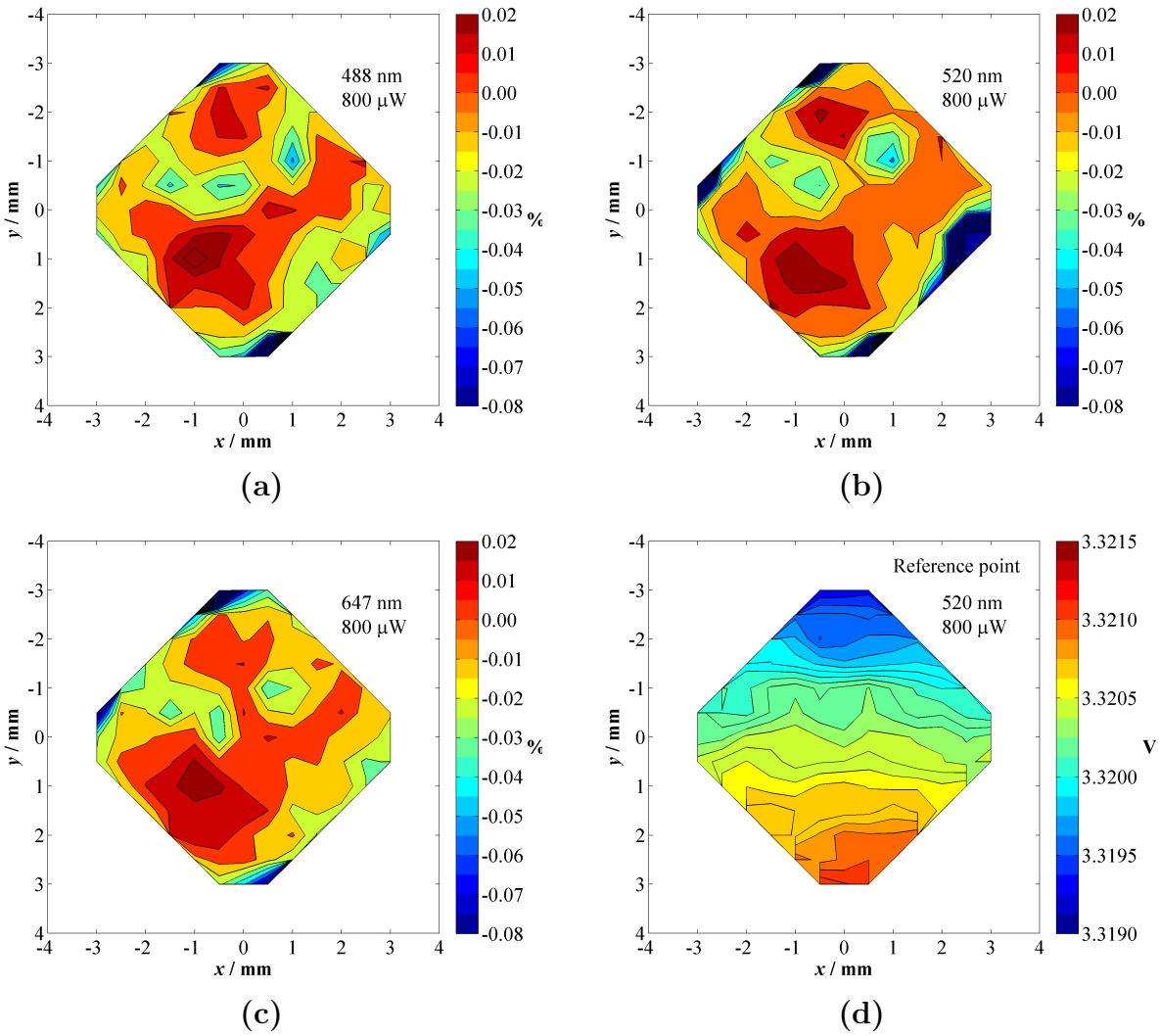

Figure 19: Spatial uniformities of the trap detector scanned with the step size of 0.5 mm at the wavelength of (a) 488 nm, (b) 520 nm and (c) 647 nm. Figure (d) shows, how the center point varied during the 520 nm scan of the trap detector. The signal amplitude of the reference point changed due to the fluctuations of the beam power.

5.2 Comparison of a pyroelectric radiometer against a trap detector

Absolute power responsivity of the pyroelectric radiometer (Rk-5720 with detector RkP-575) was calibrated against the trap detector (UVFR-8). Both detectors were introduced earlier in the document.

The trap detector used as the reference has been calibrated against another trap

detector traceable to a cryogenic electrical substitution radiometer at SP (Technical Research Institute of Sweden) [27]. The results presented in this section were also documented in a Calibration certificate [28].

An intensity-stabilized $KrAr^+$ laser at the wavelength of 488 nm with a beam diameter of about 1 mm ($1/e^2$) was used as the radiation source. The detectors were aligned perpendicular to the laser beam and centered.

In this calibration, the same measurement devices were used and they were connected in the same way as described in Chapter 5.1. Measurement was repeated 5 to 10 times and the results were averaged. The pyroelectric radiometer has a display that shows directly the measured power. It has also an analog voltage output used in automated measurements when logging the signal with computer. In this calibration, the measurement results were taken from the analog output. The correspondence between the display and the analog output of the pyroelectric radiometer was calibrated separately. The results are shown in Table 4.

Table 4: Correspondence between the display and the analog output power of the pyroelectric radiometer measured at the wavelength of 633 nm with power levels of 40–100 µW. The uncertainty stated is the relative standard deviation of the results.

Range	0–200 µW	0–2 mW	0–20 mW
Correction	1.0013 ±0.0015	1.0022 ±0.0028	0.9939 ±0.0102

The multimeter was set to the DC voltage mode of 10 V with the integration time of 100 ms and the responses of all detectors were measured with it. The ranges of 0–200 µW, 0–2 mW and 0–20 mW of the pyroelectric radiometer were calibrated using the power levels of 150 µW, 800 µW and 7.5 mW, respectively. When the range of 0–20 mW was calibrated, a ND-filter (Thorlabs NE20B) with optical density of 2 was used in front of the reference detector. The pre-amplification of the current-to-voltage converter was set to 10^4 V/A for the 150 µW and 800 µW levels and 10^5 V/A for the 7.5 mW level when calibrating Detector 1. In the case of Detector 2, the pre-amplification was set to 10^5 V/A for the 150 µW level, 10^4 V/A for the 800 µW level and 10^5 V/A for the 7.5 mW level.

Tables 5 and 6 give the correction factors for the absolute power responsivities for the pyroelectric radiometer heads at the wavelength of 488 nm with the beam diameter of 1 mm. Since the pyroelectric radiometer is spectrally flat (0.5 %) within 250 nm – 16 µm, the calibrations are valid in that range [25].

Table 5: Correction factors for the pyroelectric radiometer head Detector 1 at the wavelength of 488 nm with the beam diameter of 1 mm.

Range of the Rk-5720	Laser power / mW	Power measured with Rk-5720 / mW	Correction factor	Uncertainty ($k = 2$) / %
0–200 µW	0.1531	0.1433	1.068	3.36
0–2 mW	0.8090	0.7784	1.039	2.09
0–20 mW	7.396	7.189	1.029	2.91

Table 6: Correction factors for the pyroelectric radiometer head Detector 2 at the wavelength of 488 nm with the beam diameter of 1 mm.

Range of the Rk-5720	Laser power / mW	Power measured with Rk-5720 / mW	Correction factor	Uncertainty ($k = 2$) / %
0-200 µW	0.1524	0.1397	1.091	1.29
0-2 mW	0.8035	0.7683	1.046	1.36
0-20 mW	7.481	7.391	1.012	2.44

The uncertainty budget of the absolute responsivity calibration is given in Table 7. The uncertainty component arising from the spatial non-uniformity of the pyroelectric radiometer has been estimated as the standard deviation of the responsivities within a circle with a diameter of 1 mm in the center of the radiometer. The spatial non-uniformity leads also to another uncertainty component due to the uncertainty in beam alignment, which has been estimated as the standard deviation of the responsivities within a circle with a diameter of 1 mm in the center of the radiometer, see Table 9. Uncertainty components arising from the non-linearity of less than 1 % and the spectral flatness of 0.5 % are not included in the uncertainty budget [25]. These have to be taken into account separately when measuring with the device using different wavelengths and different power levels as compared to this calibration.

Table 7: Uncertainty budget of the absolute power responsivity calibration.

Component	Standard uncertainty / %		
	0–200 µW	0–2 mW	0–20 mW
Calibration of the trap detector		0.051	
Spatial responsivity within a circle of 1 mm in diameter*		1.000 / 0.549	
Calibration of the multimeter		0.002	
Calibration of the CVC		0.004	
Resolution of the analog output of the pyroelectric radiometer	0.0019	0.0036	0.0038
Correspondence between the display and the analog output	0.150	0.280	1.025
σ_M of the filters*	–	–	0.0017 / 0.0308
σ_M of the measurements*	1.342 / 0.295	0.123 / 0.279	0.241 / 0.365
Combined standard uncertainty*	1.681 / 0.643	1.047 / 0.679	1.453 / 1.220
Expanded uncertainty ($k = 2$)*	3.362 / 1.286	2.094 / 1.357	2.906 / 2.440

* Detector 1 / Detector 2

The poor spatial uniformity of the detectors shown in Figure 18 can be corrected if the size of the beam is known. Correction factors in Table 8 were calculated from the spatial uniformities in Figure 18. They can be applied to the results when measuring laser beams with diameters larger than the 1 mm beam used in the calibration.

Table 8: Correction factors for measuring beams with diameter larger than 1 mm with the pyroelectric radiometer heads.

Diameter / mm	Correction factor	
	Detector 1	Detector 2
<1	1.0000	1.0000
1	1.0017	1.0027
2	1.0030	1.0064
3	1.0061	1.0109
4	1.0088	1.0139
5	1.0117	1.0165
6	1.0136	1.0180
7	1.0148	1.0193
8	1.0162	1.0208
9	1.0169	1.0223
10	1.0210	1.0276
11	1.0532	1.0526
12	1.1621	1.1133

Spatial uniformity introduces additional uncertainty due to the uncertainty in beam alignment. Table 9 gives relative standard deviations of the responsivities over the area of the pyroelectric radiometer heads for various diameters. These values can be used to obtain uncertainty if the alignment accuracy of the laser is known.

Table 9: Standard deviations of the responsivities of the pyroelectric radiometer heads within a circle of the pointed diameter.

Diameter / mm	Uncertainty / %	
	Detector 1	Detector 2
1.0	1.000	0.549
1.5	1.220	0.633
2.0	1.266	0.700
2.5	1.394	0.748
3.0	1.493	0.816
3.5	1.622	0.837
4.0	1.709	0.857
4.5	1.834	0.892
5.0	1.902	0.931
5.5	1.985	0.981
6.0	2.041	1.020

5.3 Yellowness indices of polystyrene samples

The setup developed was used to study polystyrene photoyellowing. The polystyrene samples were degraded by exposing them to UV radiation using a spectrograph developed by Kärhä *et al.* presented in Figure 20 [5, 6]. The spectrograph separates light from a lamp to spectrally resolved UV radiation. It is based on a 1 kW xenon (Xe) lamp and a flat-field concave holographic grating. The grating disperses the light at the wavelength range of 276–421 nm onto the sample plane of 17 cm × 1.5 cm. The outer dimensions of the samples studied are 19 cm× 3.0 cm.

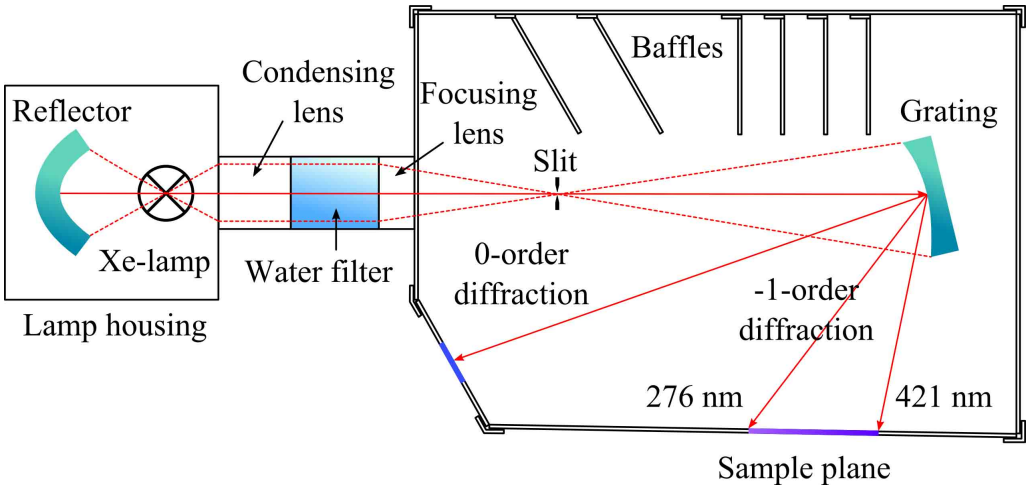

Figure 20: Structure of the UV spectrograph (redrawn) [5].

The spectrum of the xenon lamp changes as a function of the ageing time. The irradiation level decreases, decreasing being fastest at the lower wavelengths. The xenon lamp is replaced after usage of 1000 h. Ageing of the lamp is taken into account by measuring the irradiation levels at eight points in the sample plane. Thus, ageing of the samples are comparable both as a function of the exposure wavelength and as a function of the UV dose.

The polystyrene samples, in Figure 21, were exposed to UV radiation by different time periods selected as powers of 2 ranging from 2 to 256 hours.

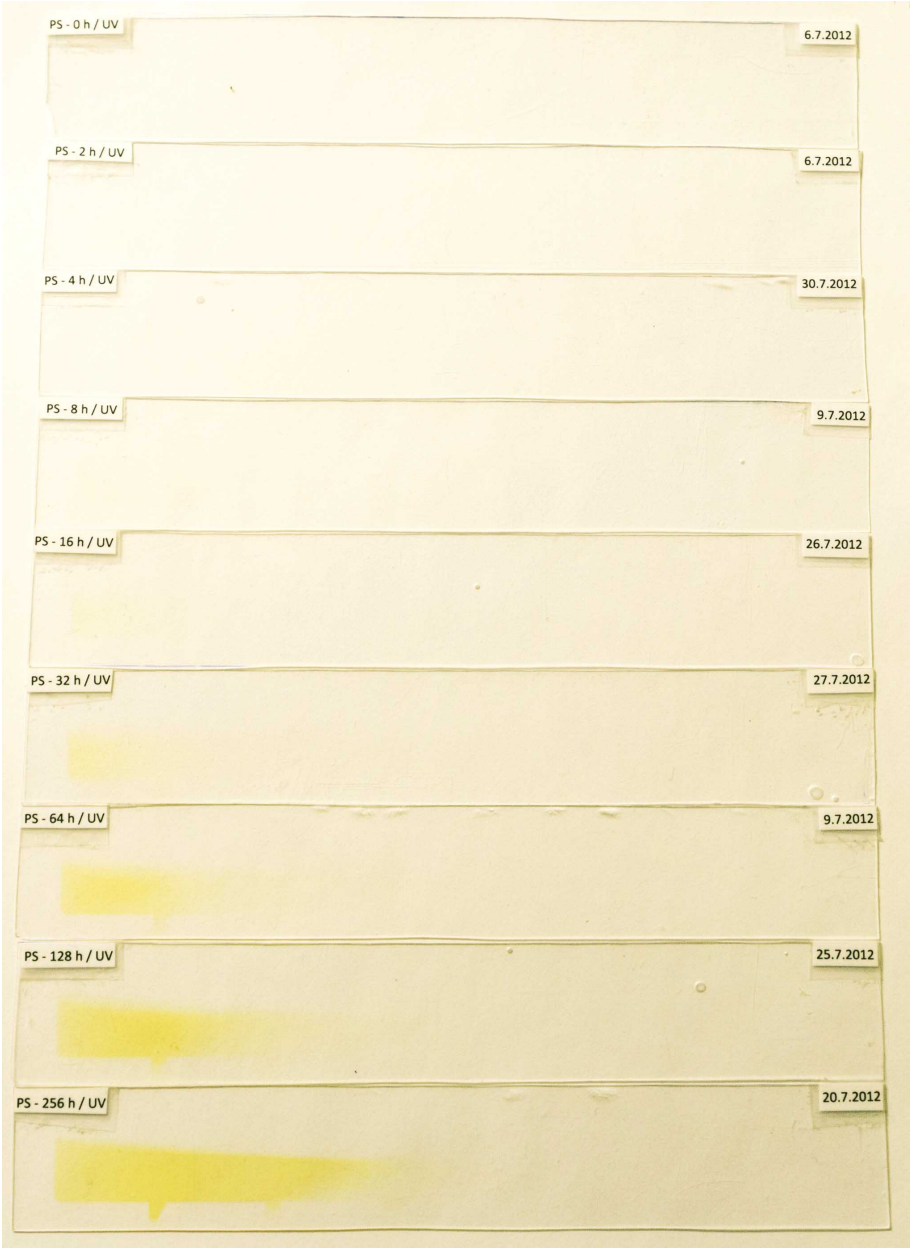

Figure 21: UV degraded polystyrene samples.

The UV dose (kJ m^{-2}) for each sample and location was calculated as

$$D = \iint E(\lambda_e)\mathrm{d}\lambda_e\mathrm{d}t\,, \tag{13}$$

where $E(\lambda)$ is the irradiance (mW m^{-2} nm^{-1}), t is the exposure time (s) and λ_e is the exposure wavelength (nm). The bandwidth of 1 nm and the average irradiation measured in the beginning and in the end of the ageing were used for calculating the UV doses.

The total UV doses for each aged sample are shown in Figure 22. As seen, the UV dose varies as a function of wavelength. Moreover, the UV dose around 280 nm does not increase systematically. The samples at 2 h, 8 h, 64 h and 256 h were aged using a new xenon lamp, whereas with the others, the lamp was already aged.

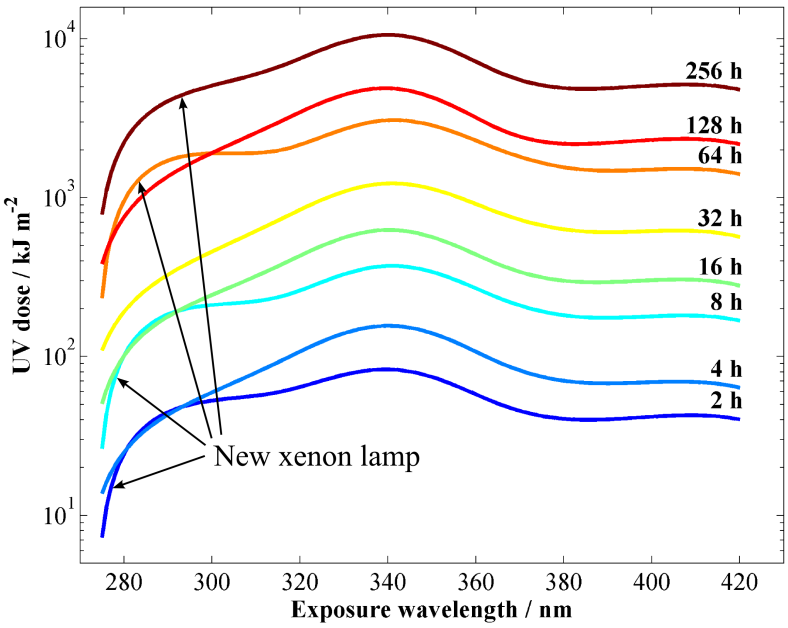

Figure 22: UV dose of each exposed polystyrene sample.

The horizontal positions x (mm) measured from the left edge of the samples has to be converted to exposure wavelengths λ_e (nm) to see how the exposure wavelength will affect the UV degradation [5]. The correspondence was empirically determined by fitting a polynomial (Red curve) to the measured exposure wavelengths (Black dots) in Figure 23. The obtained correspondence is thus

$$\lambda_e(x) = -0.0006x^2 + 0.9968x + 262.76\,. \tag{14}$$

By deriving equation (14), the reciprocal linear dispersion (nm / mm) is obtained as

$$\frac{\mathrm{d}\lambda_e(x)}{\mathrm{d}x} = -0.0012x + 0.9968\,. \tag{15}$$

Thus, scanning the sample with the beam diameters of 1.0–1.6 mm leads to maximum spectral convolution of ∼1.3 nm.

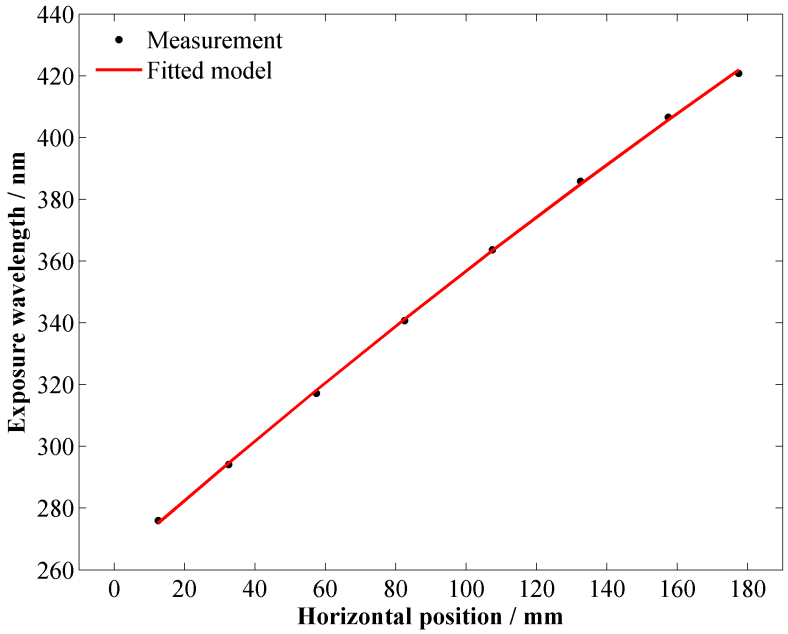

Figure 23: In the spectrograph, the horizontal sample plane position x (mm) corresponds to the exposure wavelength λ_e (nm).

The polystyrene turns yellow when exposed to UV radiation. The ageing behavior seems rather similar to newsprint whose UV-ageing properties have been researched and modelled previously [4]. The model reported uses yellowness index defined in equation (7) as a measure of the damage level caused by UV light. Based on this previous research, the damage level of polystyrene is also quantified with the yellowness index in this research.

The aged polystyrene samples were attached one at a time to the sample holder unit of the laser-based measurement setup. The transmitted beam was measured with the integrating sphere with the photodiode detector. The current of the photodiode detector was converted to voltage (FEMTO DDPCA-300) before measuring it with a multimeter (Agilent 34401A) to preserve linearity of the detector output. The samples were then scanned horizontally with 1-mm interval to get transmittances at various locations of the samples corresponding to different exposure wavelengths.

To see how equally the spectrograph actually ages the sample plane, the polystyrene sample aged for 256 h was horizontally scanned at the measurement wavelength of 476 nm with the resolution of 5 mm at various heights. The result is shown in Figure 24. As can be seen, the ageing varies upto 10 % in the vertical

direction. Therefore, a vertical position of 18 mm from the upper edge of each sample was selected to be constant for further measurements.

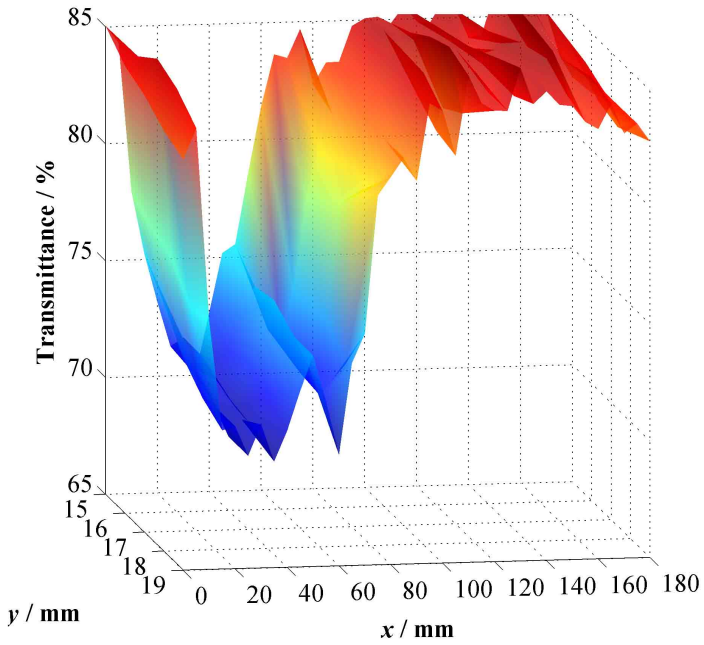

Figure 24: Transmittance of the 256 h aged polystyrene sample was spatially scanned at the wavelength of 476 nm with the resolution of 5 mm at vertical heights of 15 mm, 16 mm, 17 mm, 18 mm and 19 mm from the upper edge.

Figure 25 shows transmittances of the polystyrene sample aged for 256 h. The transmittances were scanned at various laser wavelengths. The transmittances measured at 476–568 nm drop at the exposure wavelength range of 276–340 nm due to the UV-induced photoyellowing. Surface of the sample has scratches causing systematic deviation in the transmittance level regardless of the measurement wavelength.

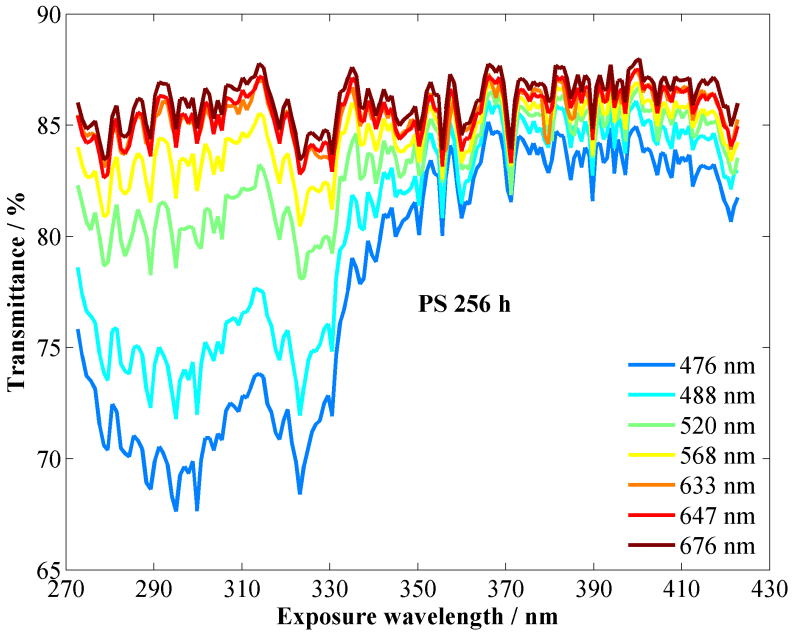

Figure 25: Transmittances of the polystyrene sample aged for 256 h were scanned horizontally using seven laser wavelengths.

Figure 26 shows the same scanning results, but the effect of the scratches has been corrected by normalizing the transmittances with respect to the transmittance measured with the 676 nm laser beam. The same process was conducted for transmittances of the samples aged for 128 h and 0 h presented in Figures 27 and 28.

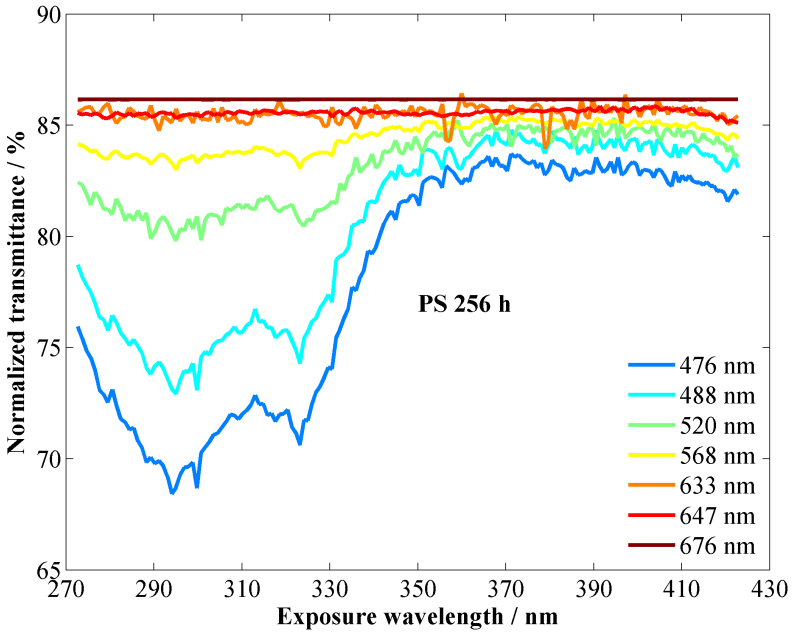

Figure 26: Normalized transmittances of the polystyrene sample aged for 256 h. Effect of the scratches has been corrected by normalizing the transmittances with respect to the transmittance measured with the 676 nm laser beam.

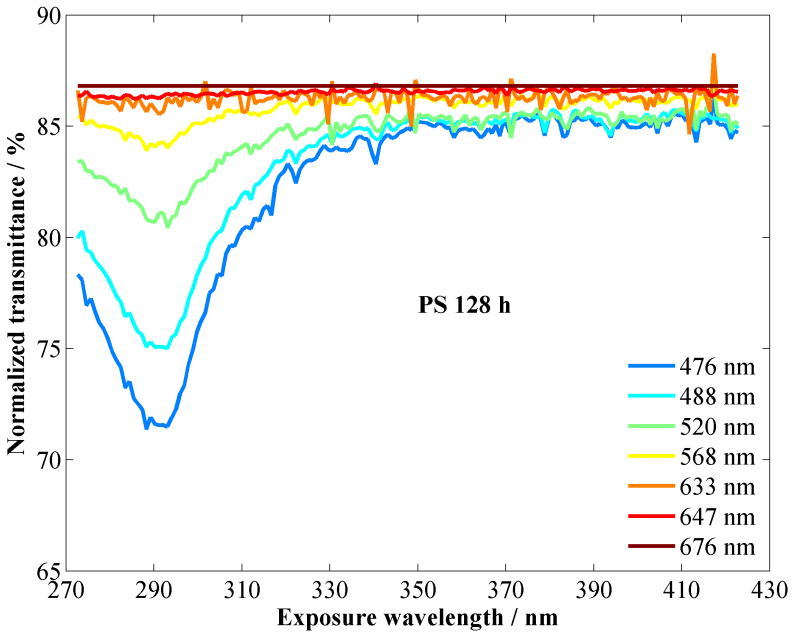

Figure 27: Normalized transmittances of the polystyrene sample aged for 128 h.

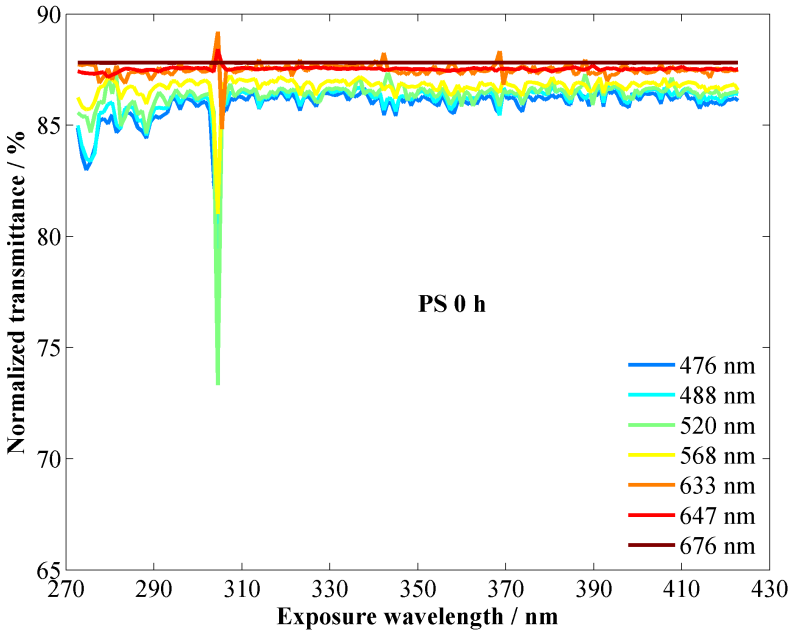

Figure 28: Normalized transmittances of the non-aged polystyrene sample show the baseline of the transmittances.

Standard illuminant D65 was selected as the light source meaning the calculated color coordinates correspond to the color perceived by us under natural daylight. Both the color matching function data and the standard illuminant D65 data cover the visible spectrum of 380–780 nm with the step size of 5 nm. All scanned points of each measured sample were measured using seven wavelengths from 476 nm to 676 nm. To be able to calculate the tristimulus values of the XYZ color space in practice, the transmittance spectrum has to be known with 5-nm step size.

Resulting from the lack of the measurement points, the polystyrene samples aged for 0 h and 256 h were measured at five different locations using a lamp-based spectrophotometer (Perkin Elmer Lambda 900) in order to verify the shape of the polystyrene transmittance spectrum as shown in Figure 29. The measurements carried out using the spectrophotometer cover the wavelength range of 325–800 nm with a step size of 1 nm. Based on the spectra measured with the spectrophotometer, an experimental function of

$$T(\lambda) = -\frac{a}{(\lambda - b)^5} + c\,, \tag{16}$$

was fitted to the seven data points. Here, parameters a, b and c are constants and λ is the measurement wavelength. Because the whole visible spectrum was not

covered with the data, the fitting was challenging. The function was fitted to the seven transmittance points measured using laser. The fitting was carried out for each measured position of the scanned polystyrene samples. Both transmittances measured with the laser and with the Perkin Elmer Lambda 900, as well as the fitted curves based on equation (16), are presented in Figure 29.

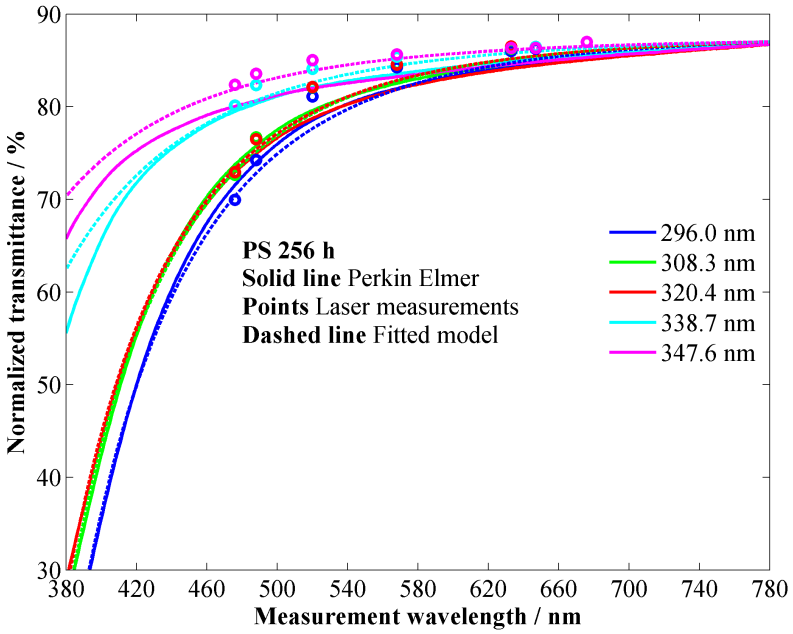

Figure 29: Transmittance spectra of the polystyrene sample aged for 256 h were measured using the Perkin Elmer Lambda 900 (Solid lines) with a step size of 1 mm and using the laser-based measurement setup (Points). Experimental function was fitted to the measurement points (Dashed lines). Line colors indicate the exposure wavelength. All the curves are normalized to 87 % at the measurement wavelength of 780 nm.

Finally, the yellowness indices shown in Figure 30 were calculated from the transmittance spectra presented in Figures 26–28 for three polystyrene samples.

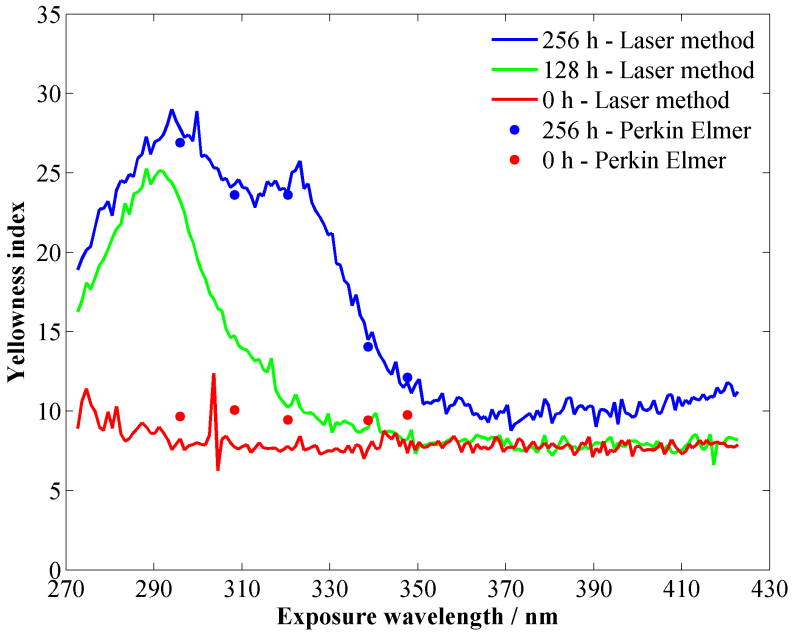

Figure 30: Yellowness indices calculated using the fitted transmittance spectra (Solid lines) and yellowness indices calculated using the transmittance spectra measured with the Perkin Elmer (Points). The analysis was carried out for three polystyrene samples aged for 256 h, 128 h and 0 h. The results from the Perkin Elmer are presented in order to validate the method.

6 Laser safety

Abuse of lasers may cause safety accidents involving eye injuries. At the worst, eyesight may be lost permanently. In addition to the eye injuries, exposing skin for long times to the UV radiation may cause skin burn which can in the long run lead to cancer. In order to improve laser safety, lasers are classified to the safety classes based on their dangerousness by IEC (International Electrotechnical Commission) [7]. This chapter introduces typical injuries caused by lasers, the international laser safety classification and how the safety issues are taken into account in this thesis.

6.1 Injuries caused by lasers

Eye injuries are the most typical consequences of the laser accidents which can lead at the worst to blindness. Skin burn is also possible with very high powers. If the skin is exposed long times to UV radiation, exposure can lead to cancer. The typical pathological effects caused by excessive exposure to light are listed in Table 10 as a function of the spectral region, as defined by CIE. Photokeratitis, also known as snow blindness, is a temporal loss of the eyesight that is caused by ultraviolet (C) light [29]. Cataract means clouding of the lens, and aqueous flare means turbidity of the aqueous humor caused by increased protein levels and cells [30, 31].

Table 10: Pathological effects associated with excessive exposure to light listed in the IEC 60825-1 standard [7].

<table>
<tr><th>CIE Spectral region</th><th>Eye</th><th colspan="2">Skin</th></tr>
<tr><td>Ultraviolet C
(180 nm to 280 nm)</td><td rowspan="2">Photokeratitis</td><td rowspan="2">Erythema (sunburn)
Accelerated skin ageing
Increased pigmentation</td><td rowspan="2"></td></tr>
<tr><td>Ultraviolet B
(280 nm to 315 nm)</td></tr>
<tr><td>Ultraviolet A
(315 nm to 400 nm)</td><td>Photochemical cataract</td><td rowspan="2">Pigment darkening
Photosensitive reactions</td><td rowspan="5">Skin burn</td></tr>
<tr><td>Visible
(400 nm to 780 nm)</td><td>Photochemical and thermal retinal injury</td></tr>
<tr><td>Infrared A
(780 nm to 1.4 µm)</td><td>Cataract
Retinal burn</td><td rowspan="3"></td></tr>
<tr><td>Infrared B
(1.4 µm to 3.0 µm)</td><td>Aqueous flare, cataract, corneal burn</td></tr>
<tr><td>Infrared C
(3.0 µm to 1000 µm)</td><td>Corneal burn only</td></tr>
</table>

6.2 Laser classification

To improve laser safety, IEC has published an international standard IEC 60825-1 for the safe use of laser products [7]. In addition to the international standard, several countries are controlled by the internal regulations. For example, LIA (Laser Institute of America) has published an ANSI Z136.1 and STUK (Radiation and Nuclear Safety Authority Finland) gives safety instructions in Finland [8, 9]. The regulations by both authorities are based on the IEC 60825-1. IEC classifies laser devices in ascending order to the safety classes based on their dangerousness as follows.

Class 1: Lasers with weak emission that are not hazardous under reasonably foreseeable conditions of operation belong to Class 1. The accessible emission limit depends on the wavelength specified in [7]. In addition, enclosed devices with relative low-power higher order laser inside may belong to this class if the laser beam travels only inside the device. [7, 10]

Class 1M: Lasers in Class 1M emit in the wavelength range from 302.5 nm to 4000 nm. They are safe under reasonably foreseeable conditions of operation, but may be hazardous if the beam is modified with optics. Two conditions apply:

(a) for diverging beams if the user places optical components within 10 cm from the source to collimate the beam; or

(b) for a collimated beam with a diameter larger than the diameter specified in [7] for the measurements of irradiance and radiant exposure. [7, 10]

Class 2: Lasers in Class 2 emit visible radiation with maximum emission of 1 mW in the wavelength range from 400 nm to 700 nm where eye protection is normally afforded by aversion responses, including the blink reflex. However, staring directly at the beam can cause damage to the eyes. Outside the wavelength range from 400 nm to 700 nm, any additional emissions of Class 2 lasers are required to be below the accessible emission limit of Class 1. [7, 10]

Class 2M: Lasers in Class 2M emit visible radiation in the wavelength range from 400 nm to 700 nm where eye protection is normally afforded by aversion responses including the blink reflex. However, viewing of the output may be more hazardous if the beam is modified with optics. Two conditions apply:

(a) for diverging beams, if the user places optical components within 100 mm from the source to concentrate (collimate) the beam, or

(b) for a collimated beam with a diameter larger than the diameter specified in [7] for the measurements of irradiance and radiant exposure. Outside the wavelength range from 400 nm to 700 nm, any additional emissions of Class 2M lasers are required to be below the accessible emission limit of Class 1M. [7, 10]

Class 3R: Lasers in Class 3R emit in the wavelength range from 302.5 nm to 1000 µm where direct view of the beam is potentially hazardous but the risk is lower than for Class 3B lasers. The accessible emission limit is 5 mW in the wavelength range from 400 nm to 700 nm and within five times the accessible emission limit of Class 1 for other wavelengths. [7, 10]

Class 3B: Class 3B consists of lasers that exceed the accessible emission limit of Class 3R. The accessible emission limit of the continuous-wave Class 3B laser is 500 mW. Direct or mirror reflected laser beam of this class is always hazardous. However, viewing diffuse reflections is normally safe. [7, 10]

Class 4: Lasers in Class 4 are capable of producing hazardous diffuse reflections. They may cause skin injuries and could also constitute a fire hazard. Their use requires extreme caution. [7, 10]

A combination of energy content and pulse characteristics of a laser beam is described as accessible emission limit (AEL). In the most of the safety classes, the AEL varies depending on the laser wavelength. Equations for these limits are presented in detailed tables 1–4 in the IEC 60825-1.

6.3 Laser safety in this setup

As presented in Table 11, most of the lasers used as the light sources in the measurement setup belong to the safety class 3B. Therefore, safety glasses with high optical density at the operating wavelength have to be used when operating the device.

Table 11: Safety classifications of the lasers used in the setup.

Laser type	Manufacturer	Model	IEC safety classification	Appropriate safety glasses
$KrAr^+$	Melles Griot	35-KAP-431	3B	LG10 for 476–520 nm LG4 for 568–676 nm
HeNe	Thorlabs	HRP005S	2	LG4 for 633 nm
IR diode	Power Technology Inc.	IQ6	3B	LG1 or LG10 for 940 nm
HeCd [a]	Kimmon Koha Co. Ltd.	IK5551R-F	3B	LG1, LG4 or LG10 for 325 nm LG1 or LG10 for 442 nm
HeCd [b]	Melles Griot	2056-M-A02		
IR HeNe [b]	Melles Griot	25-LIP-151-230	3B	LG11 for 1523 nm (Not ordered)

[a] Will be ordered
[b] Not currently installed

Optical density describes efficiency of the protection against the laser beam, and it is defined in equation (11). Higher OD indicates better protection against the laser beam. For example, OD of 5 means that only 0.001 % of the beam is transmitted through the safety glasses. However, safety glasses with this high OD cannot typically be used when aligning the beam, because the beam cannot be seen at all.

Four different laser safety glasses of Thorlabs were selected to be used when operating with the measurement setup. Their optical densities are shown in Figure 31.

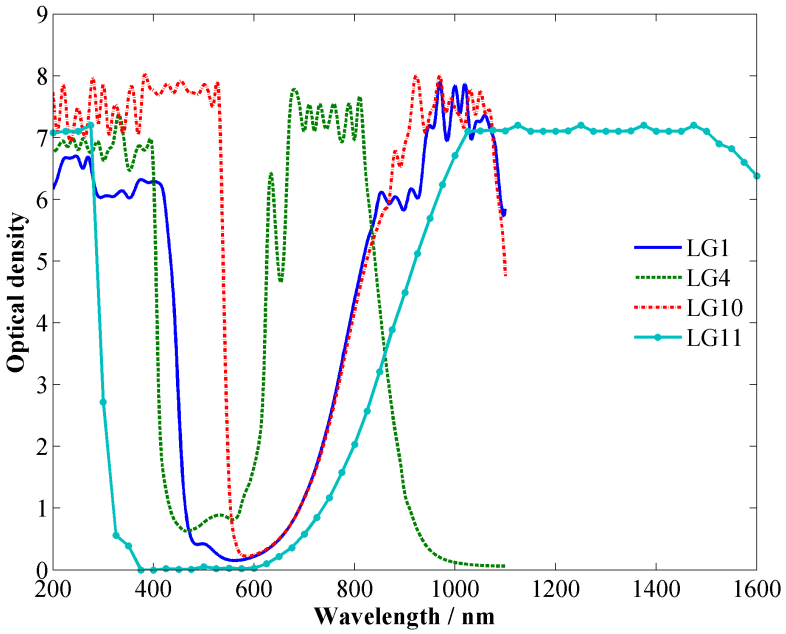

Figure 31: Optical densities of four laser safety glasses of Thorlabs.

In the case of UV and IR lasers, special alignment tools, such as laser viewing cards have to be used when aligning the beam. Light-sensitive area of these cards emits the absorbed non-visible light as visible light. Materials used in the cards define their spectral properties. Cards are typically made of plastic with a photosensitive region, as shown in Figure 32, or metal with a liquid-crystal film. [32] In principle, aligning such laser beams with the help of aligning tools is safe because one can fully protect oneself against the wavelength of the invisible beam, but still see its location on the card.

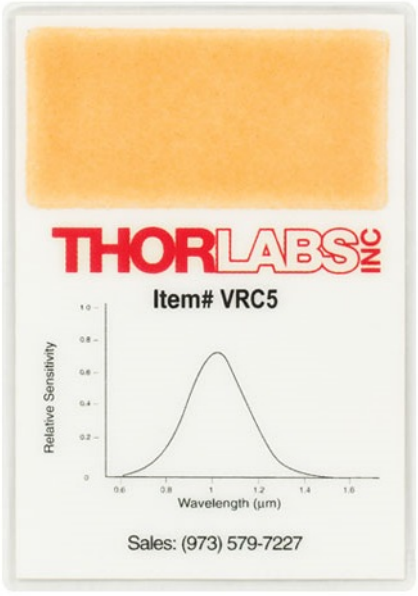

Figure 32: Laser viewing card (VRC5) is used with the safety glasses (LG10) when aligning the IR diode laser at 940 nm. The absorption band of the card is 700–1400 nm.

7 Conclusions

In this research, a laser-based setup for characterizing optical detectors and materials was designed and constructed. The setup contains multiple lasers that can be selected with a moving mirror. The sample plane provides interchange of detectors and spatial scan of detectors and transparent materials.

The setup was characterized by measuring the laser beam quality. The long-term stability of the laser beam varies upto 0.05 % with a relative standard deviation of 0.01 % when using the laser power controller. Without the controller, the beam varies by 27 %. By monitoring the stabilized beam with a monitor detector, the relative standard deviation was measured to decrease below 0.007 %. The spatial filter was verified to smooth the spatial intensity distribution, especially with diode lasers.

Test measurements conducted with the setup consisted of measuring two optical detectors for their spatial uniformities, and scanning spatially the transmittance spectra of UV degraded polystyrene samples.

In the detector measurements, the uniformity of the 3-element Si-trap detector was within 0.1 %. With the pyroelectric radiometer, the spatial responsivity varied by approximately 10 % for two detector heads, Detector 1 and Detector 2. The absolute power responsivities of the detector heads of the pyroelectric radiometer were calibrated at the wavelength of 488 nm with the power ranges of 0–200 µW, 0–2 mW and 0–20 mW against a traceable trap detector. The obtained uncertainties for Detector 1 were 3.36 % at 0–200 µW, 2.09 % at 0–2 mW and 2.91 % at 0–20 mW ranges. The corresponding uncertainties for Detector 2 were 1.29 %, 1.36 % and 2.44 %, indicating that Detector 2 is in better condition. Since the pyroelectric radiometer is spectrally flat within 250 nm – 16 µm, the calibration is valid over a wide wavelength range.

In the transmittance measurements, eight polystyrene samples were first exposed to UV radiation of 276–421 nm for different time periods using a spectrograph. The transmittance spectra of three samples were then scanned at seven laser wavelengths within 476–676 nm to demonstrate the potential of the method for quantifying photoyellowing of materials with yellowness index. The yellowness indices for the polystyrene samples were derived from the scanned transmittance spectra. Based on the results, the UV-induced photoyellowing is highest at the exposure wavelength range of 276–340 nm. The lower the measurement wavelength, the higher the absorption is, as can be expected with yellowing.

To improve the setup and to automate it further, the optical rail used for moving the laser selecting mirror could be replaced with a similar motorized translation stage as used in the XY translation stage. The manual micrometer screw for selecting the wavelength of the $KrAr^+$ laser could also be motorized. In addition, a separate multimeter for the monitor detector would enable simultaneous measurements of the response and the reference response, which would improve the compensation for the beam fluctuation.

In the future, I will measure the transmittance spectra of the rest of the polystyrene samples to derive the action spectrum of polystyrene photoyellowing. A dual-wavelength HeCd laser (Kimmon Koha IK5551R-F) will be installed in the setup to increase the reliability of the method enabling to measure transmittances at 325 nm and 442 nm, thus covering larger part of the visible spectrum.

The setup developed improves significantly the quality of detector calibrations in the Metrology Research Institute. Automated determination of the center of the detector improves accuracy and repeatability of consecutive annual calibrations. The setup also enables routine scanning of the spatial uniformity in pursuance of the calibration, which can be used to check the condition of the detector. Dust is a serious issue with high-accuracy calibrations which can now be identified. In the material science, a combination of the UV spectrograph and the new laser-based measurement setup enables a novel method for studying the UV-induced aging of transparent materials with a resolution smaller than 2 nm, which is a significant improvement for earlier methods.

References

[1] M. Sildoja, *Predictable Quantum Efficient Detector*, Doctoral Dissertation (Metrology Research Institute, Aalto University School of Electrical Engineering, Espoo, Finland, 2013) ISBN: 978-952-60-5462-9, 115 p.

[2] ASTM D1925–70, *Standard Test Method for Yellowness Index of Plastics*, (American Society for Testing and Materials, Philadelphia, United States of America, Reapproved 1988) 3 p.

[3] A. L. Andrady, S. H. Hamid, X. Hu and A. Torikai, "Effects of increased solar ultraviolet radiation on materials," *J. Photochem. Photobiol., B* **46**, 96–103 (1998).

[4] A. Heikkilä and P. Kärhä, "Photoyellowing revisited: Determination of an action spectrum of newspaper," *Polym. Degrad. Stabil.* **99**, 190–195 (2014).

[5] A. Sormanen, *Spektrinen ikäännytyslaitteisto lämmitettäville materiaalinäytteille*, Special Assingment of Measurement Science and Technology (Metrology Research Institute, Helsinki University of Technology, Espoo, Finland, 2009) 20 p.

[6] P. Kärhä, A. Heikkilä, K. Ruokolainen and M. Kaunismaa, "A novel facility for ageing materials with narrow-band ultraviolet radiation exposure," *Rev. Sci. Instrum.* **82**, 023107-1–023107-6 (2011).

[7] IEC 60825-1: 2001-08, *Safety of laser products – Part 1: Equipment classification, requirements and user's guide*, 1.2 Edition (International Electrotechnical Commission, Geneva, Switzerland, 2001) pp. 19, 28–29 and 98, 122 p.

[8] ANSI Z136.1: 2007-03, *American National Standard for Safe Use of Lasers* (Laser Institute of America, Orlando, United States of America, 2007) 249 p.

[9] Web-sites of STUK (cited: Feb. 18$^{\text{th}}$ 2014) available: `http://www.stuk.fi`

[10] STUK, "Lasers" (cited: Feb. 18$^{\text{th}}$ 2014) available: `http://www.stuk.fi/sateilyn-hyodyntaminen/laserit/en_GB/laser/`

[11] F. L. Pedrotti, S. J. and L. S. Pedrotti, *Introduction to Optics*, 2$^{\text{nd}}$ Edition (Prentice-Hall, Englewood Cliffs, United States of America, 1993), pp. 102–105, 307, 310–312, 426 and 440–444, ISBN: 0-13-016973-0, 602 p.

[12] C. C. Hoyt and P. V. Foukal, "Cryogenic Radiometers and their Application to Metrology," *Metrologia* **28**, 163–167 (1991).

[13] K. Venkataraayan, S. Askraba, K. E. Alameh and C. L. Smith, "Photonic-based multi-wavelength sensor for object identification," *Opt. Express* **18**, 3774–3783 (2010).

[14] Thorlabs, "Beam splitters" (cited: Mar. 4th 2014) available: `http://www.thorlabs.de/navigation.cfm?guide_id=2240`

[15] Melles Griot, "Introduction to Laser Technology," Technical Guide, pp. 10.6–10.8 (2009).

[16] F. J. Duarte, *Tunable Laser Applications*, 2nd Edition (CRC Press, New York, United States of America, 2009), pp. 248 and 264, ISBN: 978-1-4200-6009-6, 480 p.

[17] U. Minoni, G. Manili, S. Bettoni, E. Varrenti, D. Modotto and C. De Angelis, "Chromatic confocal setup for displacement measurement using a supercontinuum light source," *Opt. Laser Technol.* **49**, 91–94 (2013).

[18] Thorlabs, "Beam Analyzing Software BP209 Operation Manual," Operation Manual, Rev. 5.0.2 (2013).

[19] BEOC, "Laser Power Controller," Operation Manual, Rev. 5.2 (2006).

[20] T. Kübarsepp, A. Haapalinna, P. Kärhä ja E. Ikonen, "Nonlinearity measurements of silicon photodetectors," *Appl. Opt.* **37**, 2716–2722 (1998).

[21] T. Kübarsepp and M. White, "Ten-element photodetector for optical power and attenuation measurements," *Appl. Opt.* **49**, 3774–3779 (2010).

[22] CIE, "Selected Colorimetric Tables" (cited: Feb. 18th 2014) available: `http://www.cie.co.at/index.php/LEFTMENUE/index.php?i_ca_id=298,CIE1931`

[23] T. Erdogan, "How to calculate luminosity, dominant wavelength, and excitation purity," *Semrock White Paper Series*, 2–3 (2013).

[24] D. R. Malinin and J. H. Yoe, "Development of the Laws of Colorimetry: A historical sketch," *J. Chem. Educ.* **38**, 129–131 (1961).

[25] Laser Precision Corp., "Rk-5700 Series Operating Instructions," Operation Manual, Rev. C, 1989.

[26] N. P. Fox, "Trap Detectors and their Properties," *Metrologia* **28**, 197–202 (1991).

[27] T-R 766, *Calibration certificate – Responsivity of 6 working standard trap detectors* (Metrology Research Institute, Espoo, Finland, Sept. 27$^{\text{th}}$ 2012) 4 p.

[28] T-R 822, *Calibration certificate – Pyroelectric radiometer* (Metrology Research Institute, Espoo, Finland, Nov. 26$^{\text{th}}$ 2013) 5 p.

[29] H. R. Taylor, "The biological effects of UV-B on the eye," *Photochem. Photobiol.* **50**, 489–492 (1989).

[30] D. Allen and A. Vasavada, "Cataract and surgery for cataract," *Brit. Med. J.* **333**, 128–132 (2006).

[31] O. M. Guillén-Monterrubío, J. Hartikainen, K. Taskinen and K. M. Saari, "Quantitative determination of aqueous flare and cells in healthy eyes," *Acta Ophthalmol. Scand.* **75**, 58–62 (1997).

[32] Thorlabs, "Laser alignment tools" (cited: Feb. 18$^{\text{th}}$ 2014) available: `http://www.thorlabs.de/navigation.cfm?guide_id=2324`